Mesoscale Matter as Constrained Field Dynamics

A Unified Framework for Structure, Transport, and Function

Flyxion
Independent Researcher

May 3, 2026

Abstract

We propose a unified mathematical framework for constrained field dynamics, applicable across soft matter physics, biophysics, nanotechnology, materials engineering, and cosmology. Systems are represented through a coupled field encoding structural constraint, directed transport, and configurational accessibility — the latter measuring the local logarithmic volume of admissible future trajectories. At the mesoscale, variational free-energy functionals and dissipative evolution equations show that self-assembly, phase transitions, anisotropy, and structure-dependent transport arise as natural consequences of this coupling. Functional systems are characterized as those whose trajectories enter and remain within low-accessibility basins, where configurational options have collapsed and dynamics become reproducible.

The trajectory-aware representation is formalized using sheaf theory. The configuration sheaf encodes local field data, Čech cohomology measures gluing obstruction, and system history is presented as a composable path in the infinity-groupoid of configurations. Accessibility collapse corresponds to truncation to a 1-sheaf, and in the fully collapsed limit geometric bundle structure emerges as the terminal descent object of constraint. We show that Lorentz transformations act as sheaf automorphisms, that superluminal propagation is categorically obstructed by the gluing condition, and that spatial variation in the constraint field induces an effective metric recovering general relativity in the appropriate limit.

Extensions to socio-technical systems formalize modular externalization and residue reuse as constraint redistribution. Connections to learning theory identify recency weighting as a minimal gluing obstruction estimator, explaining why locality constraints enable large-scale learning. A five-dimensional Ising synchronization model is proposed as a cosmological extension, generating flat galaxy rotation curves, filamentary structure, and gravitational lensing from coherence dynamics rather than particulate dark matter.

The unifying result is that persistent low configurational accessibility, reduction in admissible homotopy classes, vanishing higher sheaf cohomology, and emergence of a bundle description are equivalent signatures of functional lock-in across all domains treated in the paper.

1. Introduction: The Illusion of Disciplinary Boundaries

Scientific descriptions of matter at intermediate scales are historically partitioned across multiple disciplines. Emulsions and surfactant systems are studied within colloid science; protein aggregation and membrane organization within biophysics; polymer networks and gels within soft matter physics; nanoparticle assemblies within nanotechnology; and transport-active structures within materials engineering. Each domain employs its own vocabulary, models, and experimental techniques.

Despite this fragmentation, a common set of phenomena recurs across all of these systems: aggregation into mesoscale structures, the formation of diffuse interfaces, anisotropic alignment under external forcing, and the emergence of transport properties that depend sensitively on morphology. These phenomena are typically treated as domain-specific, yet their repeated appearance across chemically distinct systems suggests a deeper structural unity.

The central claim of this work is that these systems are not fundamentally distinct, but rather represent different observational regimes of a

common class of dynamical systems. Specifically, we argue that mesoscale matter is governed by a coupled field dynamic in which three components—constraint, transport, and configurational accessibility—interact to determine both structure and function.

1.1. From Objects to Fields

Traditional descriptions of mesoscale systems often begin with discrete entities: micelles, vesicles, protein complexes, polymer chains, or nanoparticles. While useful, such descriptions obscure the fact that the relevant observables—scattering intensities, transport coefficients, mechanical responses—depend not on individual objects, but on spatial correlations and collective organization.

This motivates a shift in perspective from discrete objects to continuous fields.

Definition 1.1 (Mesoscale State)**.** *Let $\Omega \subset \mathbb{R}^d$ be a bounded domain. A mesoscale system is described by a state field*

$$\mathcal{X}(x,t) = (\Phi(x,t), \mathbf{v}(x,t), \mathcal{S}(x,t)),$$

where Φ encodes structural constraint, $\mathbf{v}$ encodes transport, and $\mathcal{S}$ encodes configurational accessibility.

This representation does not assume a specific microscopic origin. Rather, it provides an effective description at the scale where correlations are long-range but not uniform.

1.2. Three Interacting Components

The three components of $\mathcal{X}$ play distinct but coupled roles.

The scalar field Φ represents the degree to which configurations are locally constrained. High values correspond to ordered or aggregated regions, while low values correspond to disordered or weakly constrained regions. Where necessary, Φ may be generalized to a vector- or tensor-valued order parameter; the scalar case serves as the minimal representative.

The vector field $\mathbf{v}$ represents directed transport consistent with the local structure. It encodes fluxes of mass, charge, or stress that are admissible given the constraints imposed by Φ.

Configurational accessibility. The scalar field $\mathcal{S}(x,t)$ measures the local density of admissible trajectories through configuration space—equivalently, the logarithmic volume of dynamically accessible states consistent with Φ and $\mathbf{v}$ at that point. High values of $\mathcal{S}$ indicate that many future evolutions remain open; low values indicate that the system has become constrained into a narrow set of possible futures. This quantity generalizes entropy to the mesoscale, but its precise content is trajectory-geometric rather than thermodynamic.

Definition 1.2 (Configurational Accessibility Density)**.** *Let $\mathcal{P}_{x,t}$ denote the set of admissible future trajectories passing through (x,t). The configurational accessibility field is*

$$\mathcal{S}(x,t) := \log \mathrm{Vol}\big(\mathcal{P}_{x,t}\big),$$

where volume is taken with respect to a natural measure on trajectory space.

These fields are not independent. Structure constrains transport, transport modifies structure, and $\mathcal{S}$ regulates which transitions between structural states remain accessible.

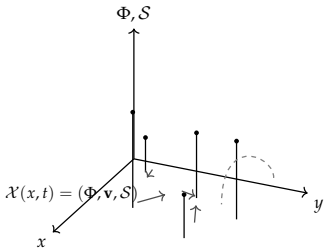

Figure 1: The mesoscale state as a coupled field: structural constraint Φ (verticals), directed transport $\mathbf{v}$ (arrows), and configurational accessibility $\mathcal{S}$ (dashed curve).

1.3. From Structure to Function

A key consequence of this coupling is that structure and function cannot be cleanly separated. In many systems, function is treated as a property layered on top of structure: a membrane filters, a polymer conducts, a nanoparticle delivers a payload. However, in each case, the observed function arises from the way the system evolves under constraint.

This leads to a reframing:

Proposition 1.3 (Function as Stabilized Dynamics)**.** *A functional mesoscale system corresponds to a regime in which the evolution of $\mathcal{X}(x,t)$ produces reproducible trajectories under fixed boundary conditions. Equivalently, functional systems occupy low-$\mathcal{S}$ regions of configuration space, where configurational accessibility has been suppressed and dynamics become reproducible.*

Proposition 1.4 (Function as Dynamical Lock-In)**.** *A system is functional on a domain $U \subset \Omega$ if and only if there exists a time interval $[t_0, t_1]$ such that $\mathcal{S}(x,t) \leq \varepsilon$ for all $x \in U$ and $t \in [t_0, t_1]$, and the induced trajectory flow is stable under admissible perturbations.*

Remark 1.5. *This condition implies that function is characterized by the suppression of trajectory diversity rather than the attainment of a particular structural state. Distinct systems with different microscopic realizations may therefore exhibit identical function if they occupy equivalent low-$\mathcal{S}$ basins.*

Thus, function is not a static attribute of structure, but the stability of dynamical evolution within a constrained configuration space. A system becomes functional not when it achieves a particular shape, but when it loses enough options that its future evolution is predictable.

1.4. Scope and Structure of the Work

The remainder of this work develops the constrained-field perspective across four broad layers: mesoscale physics, formal mathematical structure, extensions to cognition and socio-technical systems, and cosmological application.

Sections 2–6 establish the physical foundation. Section 2 formalizes the mesoscale regime and explains why neither microscopic nor continuum descriptions alone suffice. Section 3 reinterprets self-assembly as constrained selection over configuration space. Section 4 introduces the correlation-field description of structure. Section 5 shows how transport emerges from structural constraint and feeds back into it. Section 6 analyzes interfaces as active constraint boundaries whose stability arises from local suppression of $\mathcal{S}$.

Sections 7–11 develop the formal framework. Section 7 introduces trajectory-aware representation and the TARTAN patch structure, including the admissibility log as an ∞-categorical object and its variational and computational interpretations. Section 8 synthesizes these into a unified variational and dynamical framework with memory coupling and gluing constraints. Section 9 develops a homotopy-theoretic interpretation in which accessibility collapse corresponds to reduction in admissible trajectory classes. Section 10 situates the framework within high-dimensional geometry, transformer architectures, and quantum systems. Section 11 connects configurational accessibility to novelty, compression, and Schmidhuber-style intrinsic motivation.

Sections 12–17 develop the sheaf-theoretic and relativistic consequences. Section 12 formalizes the configuration sheaf, derives Čech cohomological obstructions, and shows that geometric bundle structure emerges as the terminal descent object of accessibility collapse. Section 13 establishes that Lorentz transformations act as automorphisms of the projection functor and that time dilation is projection distortion rather than physical retardation. Section 14 derives Lorentz invariance from the RSVP trajectory action. Section 15 proves that superluminal propagation is categorically obstructed by the sheaf gluing condition. Section 16 interprets time dilation geometrically. Section 17 shows how spatial variation in Φ induces an effective metric, recovering general relativity in the appropriate limit.

Sections 18–21 treat applications. Section 18 presents the collagen peptide gelation causal example. Section 19 discusses implications for material design as trajectory control. Section 20 extends the framework to modular socio-technical systems, formalizing externalization, residue reuse, and orthograde transformations. Section 21 connects recency weighting to minimal gluing obstruction estimation and explains why locality constraints enable Bitter-Lesson-style scaling.

Sections 22–28 develop the cosmological extension. Section 22 proposes a five-dimensional Ising synchronization model and derives the projection to observable RSVP fields. Section 23 derives predictions for galaxy formation, rotation curves, and environmental dependence. Section 24 constructs an effective metric from synchronization and derives lensing observables. Section 25 establishes a closure relation and forward observational pipeline. Section 26 situates the model relative to Illustris and ΛCDM simulation pipelines. Section 27 gives a comparative predictions table across ΛCDM, MOND, and the synchronization model. Section 28 presents an observational strategy for detecting field relaxation, including a no-go theorem for instantaneous gravitational response and a model-independent falsification protocol.

The paper closes with a limitations section, a conclusion, and two appendices describing algorithmic implementations of the admissibility log simulator and the cosmological synchronization forward model.

The aim throughout is not to replace existing domain-specific models, but to provide a minimal formal structure within which they can be

understood as different projections of the same constrained field dynamics.

1.5. Unified Thesis: Constrained Field Dynamics as a Cross-Scale Theory

The central thesis of this work is that systems traditionally treated as belonging to distinct domains — soft matter, biological organization, cosmology, and socio-technical networks — are in fact realizations of a common class of constrained dynamical systems. These systems are most naturally described not by discrete objects or purely continuum fields, but by the coupled evolution of structure, transport, and configurational accessibility $\mathcal{X}(x,t) = (\Phi, \mathbf{v}, \mathcal{S})$, where Φ encodes structural constraint, $\mathbf{v}$ encodes admissible transport, and $\mathcal{S}$ encodes the logarithmic volume of admissible future trajectories. The essential claim is that variation across domains does not arise from fundamentally different governing laws, but from differences in observation scale, projection, and accessibility regime.

In this framework, the apparent diversity of physical systems is reinterpreted as a diversity of projections of a common constrained field dynamic. Mesoscale matter, biological function, and cosmological structure correspond to regimes in which different components of $\mathcal{X}$ dominate or collapse. The unifying principle is that dynamical evolution is governed not only by energetic minimization but by accessibility structure: systems evolve toward regions of configuration space in which admissible trajectories are both energetically favorable and dynamically persistent.

Synthesis. The framework developed in this work unifies three perspectives: variational field dynamics, sheaf-theoretic consistency, and trajectory accessibility. These are not independent layers but different representations of the same underlying structure. The scalar field Φ encodes constraint, the vector field $\mathbf{v}$ encodes admissible motion, and the accessibility field $\mathcal{S}$ encodes the geometry of future evolution. Across all domains considered, function, structure, and stability emerge when accessibility collapses and local dynamics become globally consistent.

2. The Mesoscale Problem

The preceding discussion motivates the need for a precise characterization of the mesoscale regime. This section formalizes that regime and clarifies why it resists reduction to either purely microscopic or purely continuum descriptions.

2.1. Definition of the Mesoscale Regime

Definition 2.1 (Mesoscale Regime)**.** *A system is said to operate at the mesoscale if it satisfies the following conditions. First, its characteristic structural length ℓ satisfies $\ell_{\text{micro}} \ll \ell \ll \ell_{\text{macro}}$, where ℓ_{micro} is the scale of molecular interactions and ℓ_{macro} is the scale at which continuum averaging becomes valid. Second, two-point correlation functions $C(r) = \langle \Phi(x)\Phi(x+r) \rangle$ exhibit nontrivial structure over a finite range of r. Third, fluctuations in Φ and $\mathbf{v}$ remain dynamically relevant and are not suppressed by averaging. Fourth, the system admits a multiplicity of locally stable or metastable configurations.*

These conditions distinguish mesoscale systems from crystalline solids, where order is uniform, and from ideal gases, where correlations vanish.

2.2. Failure of Purely Microscopic Descriptions

Microscopic descriptions model systems in terms of individual particles and their interactions. While exact in principle, such descriptions become intractable for mesoscale systems due to the large number of degrees of freedom and the emergence of collective behavior. More importantly, microscopic models obscure the structures that are directly observable experimentally. Scattering experiments measure correlation functions rather than individual particle positions; the relevant variables at the mesoscale are therefore coarse-grained fields, not particle coordinates.

2.3. Limitations of Continuum Approximations

Continuum models assume that local properties vary smoothly and can be described by averaged quantities such as density or velocity. This assumption fails in mesoscale systems where interfaces, domains, and localized structures introduce sharp variations. In particular, continuum models struggle to represent diffuse interfaces between phases, coexisting domains with distinct morphologies, anisotropic structures induced by external fields, and heterogeneous transport pathways. These features require a description that retains spatial variation and correlation without reverting to full microscopic detail.

2.4. Emergent Length Scales and Pattern Formation

A defining feature of mesoscale systems is the emergence of intrinsic length scales that are not imposed externally but arise from the dynamics. Consider a scalar field Φ governed by competing energetic contributions: a local free-energy density favoring phase separation and a gradient penalty favoring smoothness. The competition between these terms generates a preferred length scale

$$\ell_* \sim \sqrt{\frac{\kappa}{|a|}},$$

where κ is the gradient coefficient and a is the quadratic coefficient in the local free-energy density. This length scale determines the size of domains, micelles, or network features, and appears across a wide range of systems.

2.5. Multiplicity of Morphologies

Mesoscale systems admit a wide range of morphologies—lamellar, cylindrical, bicontinuous, and disordered network structures—that are often observed in systems with vastly different chemical compositions, such as block copolymers, lipid membranes, and surfactant solutions. This universality suggests that morphology is determined primarily by the structure of the governing functional rather than by microscopic details.

Proposition 2.2 (Morphological Universality)**.** *Distinct physical systems governed by free-energy functionals of similar form admit qualitatively similar families of mesoscale structures.*

Heuristic Argument. If two systems share a functional of the form

$$\mathcal{F}[\Phi] = \int \left(f_{\text{loc}}(\Phi) + \kappa |\nabla \Phi|^2 \right) \, dx,$$

then their Euler–Lagrange equations are identical up to parameter values. Solutions therefore differ quantitatively but not qualitatively, leading to similar classes of structures. □

2.6. Implications for Modeling

The field representation $\mathcal{X}(x,t) = (\Phi, \mathbf{v}, \mathcal{S})$ introduced in Section 1 provides the appropriate intermediate description. It retains sufficient structure to represent interfaces, domains, and transport pathways, while abstracting away microscopic detail. In the following sections, we show how this representation naturally gives rise to self-assembly, transport, and function as emergent properties of constrained dynamics.

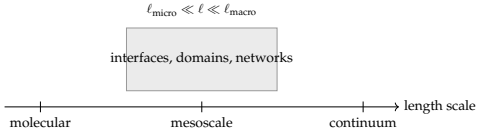

Figure 2: The mesoscale regime occupies the interval where microscopic discreteness has been coarse-grained but continuum averaging has not erased interfaces.

3. Self-Assembly as Constrained Configuration

Self-assembly is typically described as the spontaneous organization of components into structured aggregates driven by free-energy minimization. While formally correct, this description obscures a deeper mechanism: self-assembly is a process of selection over a space of admissible configurations under competing constraints.

3.1. Configuration Space and Admissibility

Let $\mathcal{C}$ denote the space of coarse-grained configurations of the system, parameterized by the structural field $\Phi(x)$. Not all elements of $\mathcal{C}$ are physically realizable; admissibility is determined by interaction energies, geometric constraints, and conservation laws.

Definition 3.1 (Admissible Configuration)**.** *A configuration $\Phi \in \mathcal{C}$ is admissible if it satisfies the constraints imposed by the system's free-energy functional and boundary conditions.*

The set of admissible configurations forms a constrained manifold $\mathcal{A} \subset \mathcal{C}$. Self-assembly is then interpreted as the evolution of $\Phi(x,t)$ within $\mathcal{A}$ toward regions that minimize the free-energy functional while remaining dynamically accessible.

3.2. Variational Structure and Energy Landscapes

The free-energy functional $\mathcal{F}[\Phi]$ induces an energy landscape over $\mathcal{A}$. Critical points correspond to stationary configurations, while local minima correspond to stable or metastable structures.

Proposition 3.2 (Self-Assembly as Gradient Flow)**.** *In the absence of external forcing, the evolution of Φ*

is governed by a gradient flow of the free-energy functional:

$$\partial_t \Phi = -\,\mathcal{G}(\Phi)\,\frac{\delta \mathcal{F}}{\delta \Phi},$$

where $\mathcal{G}(\Phi)$ is a positive mobility operator.

Remark 3.3. *This formulation generalizes classical Cahn–Hilliard and Allen–Cahn dynamics, depending on whether Φ is conserved. The specific form of $\mathcal{G}(\Phi)$ determines the kinetics but not the set of admissible equilibria.*

3.3. Competing Constraints

The richness of mesoscale structures arises from the presence of competing constraints. Typical contributions to $\mathcal{F}$ include local energetic terms favoring phase separation or aggregation, gradient penalties favoring smooth interfaces, configurational-accessibility terms favoring states with many available futures, and external fields imposing directional or spatial bias. The competition between these contributions produces nontrivial equilibria. A double-well potential combined with a gradient penalty yields phase-separated domains with finite interfacial width, while additional constraints can stabilize periodic or bicontinuous structures.

3.4. Universality of Morphological Classes

The recurrence of similar morphologies across domains—spherical micelles, cylindrical aggregates, lamellae, and bicontinuous networks in systems ranging from surfactants to block copolymers to biological membranes—follows from the shared functional form of the governing equations, not from shared chemistry.

Proposition 3.4 (Morphological Universality)**.** *If two systems are governed by free-energy functionals of similar functional form, then their sets of stable morphologies are qualitatively equivalent, differing only in scale and parameter values.*

Sketch. The Euler–Lagrange equation associated with $\mathcal{F}$ determines the stationary configurations. If the functional form of $\mathcal{F}$ is preserved, then the differential equation governing Φ is identical up to parameter scaling, and its solution set exhibits the same qualitative structure. □

3.5. The Role of Configurational Accessibility in Selection

While energy determines the location of minima in $\mathcal{F}$, the configurational accessibility field $\mathcal{S}$ determines which regions of configuration space are dynamically reachable. Regions of high $\mathcal{S}$ correspond to states from which many trajectories depart; regions of low $\mathcal{S}$ correspond to constrained states from which few escapes are available. Self-assembly therefore reflects a balance between energetic minimization and trajectory accessibility.

3.6. Aggregation as Constraint Amplification

Aggregation processes such as micelle formation or protein clustering can be interpreted as the amplification of local constraints. Initially, Φ is nearly uniform, corresponding to a weakly constrained state with high $\mathcal{S}$. As the system evolves, fluctuations drive the formation of localized regions of higher Φ, which reduce local $\mathcal{S}$ and further restrict the motion of surrounding components. This positive feedback leads to the growth of structured domains.

Proposition 3.5 (Constraint Amplification)**.** *Regions of increasing Φ locally reduce configurational accessibility, thereby promoting further aggregation through reduced mobility.*

4. Structure as a Field: Correlation, Morphology, and Stability

The previous section established that self-assembly is a constrained selection process over configuration space. We now refine this perspective by replacing the notion of discrete structure with that of a continuous field encoding spatial correlations.

4.1. From Discrete Aggregates to Correlation Fields

Experimental observations at the mesoscale do not directly resolve individual objects. Techniques such as small-angle X-ray and neutron scattering measure intensity distributions of the form

$$I(q) \;\propto\; \int_\Omega \int_\Omega \langle \Phi(x)\,\Phi(y)\rangle\, e^{-iq\cdot(x-y)}\,\mathrm{d}x\,\mathrm{d}y, \quad (1)$$

which depend on the two-point correlation function of the structural field. The primary observable is therefore not $\Phi(x)$ itself, but its statistical structure.

Definition 4.1 (Correlation Field)**.** *The correlation structure of a mesoscale system is encoded by the two-point function $C(x,y) = \langle \Phi(x)\Phi(y)\rangle$, which defines a positive semi-definite kernel on Ω.*

4.2. Effective Field Description

To obtain a tractable representation, one introduces an effective field $\Phi(x)$ whose spatial variation reproduces the observed correlations.

Remark 4.2. *This field should be interpreted as a coarse-grained order parameter rather than a literal density. Its role is to encode the degree of local structural constraint consistent with experimental observables.*

4.3. Morphology as a Solution Manifold

Morphological structures correspond to solutions of the Euler–Lagrange equation associated with the free-energy functional:

$$\frac{\delta \mathcal{F}}{\delta \Phi} \;=\; f'_{\mathrm{loc}}(\Phi) \;-\; \kappa\,\Delta\Phi \;+\; (\text{coupling terms}) \;=\; 0. \tag{2}$$

Different morphologies arise as distinct solution branches of this equation.

Proposition 4.3 (Morphological Manifold)**.** *The set of admissible morphologies forms a manifold of solutions to equation* (2)*, parameterized by system parameters such as average composition, temperature, and external forcing.*

Remark 4.4. *This perspective replaces the classification of structures by type (micelle, lamella, network) with a classification by solution branch.*

4.4. Stability and Perturbation

The stability of a given morphology is determined by the second variation of $\mathcal{F}$. A configuration Φ_0 is stable if

$$\delta^2 \mathcal{F}[\Phi_0](\psi,\psi) \;\geq\; 0 \quad \forall\, \text{admissible } \psi.$$

Proposition 4.5 (Linear Stability)**.** *Let Φ_0 be a stationary solution. Then small perturbations $\psi(x,t)$ evolve according to*

$$\partial_t \psi \;=\; -\,\mathcal{L}_{\Phi_0}\,\psi,$$

where the linearized operator is

$$\mathcal{L}_{\Phi_0} = -\,M(\Phi_0)\,\Delta\left(f''_{\mathrm{loc}}(\Phi_0) - \kappa\,\Delta\right).$$

Stability is determined by the spectrum of $\mathcal{L}_{\Phi_0}$.

4.5. Anisotropy and Broken Symmetry

Anisotropic structures induced by external fields—shear, electric fields, confinement—correspond to the breaking of rotational symmetry in Φ. This can be incorporated by introducing anisotropic gradient terms

$$\mathcal{F}_{\mathrm{aniso}}[\Phi] \;=\; \int_\Omega \frac{1}{2}\,\nabla\Phi\cdot\mathbf{K}\nabla\Phi\,dx,$$

where $\mathbf{K}$ is a positive-definite tensor whose eigenstructure determines preferred directions of alignment.

4.6. Hierarchical Structure

Many systems exhibit structure across multiple length scales. This can be modeled by extending the free-energy functional to include nonlocal terms

$$\mathcal{F}_{\mathrm{multi}}[\Phi] \;=\; \mathcal{F}[\Phi] \;+\; \int_\Omega\int_\Omega K(x-y)\,\Phi(x)\Phi(y)\,dx\,dy,$$

where K is a kernel encoding long-range interactions.

Proposition 4.6 (Multiscale Coupling)**.** *Nonlocal terms in $\mathcal{F}$ generate coupling between structures at different length scales, leading to hierarchical organization.*

5. Transport Emerges from Structure

Having established that structure is naturally described by a field $\Phi(x,t)$ encoding local constraint and correlation, we now turn to transport. Transport is not an independent degree of freedom, but emerges as constrained motion within the structural field.

5.1. Transport as Constrained Flux

In classical continuum models, transport is described by fluxes driven by gradients of potential, such as Fickian diffusion or Ohmic conduction, implicitly assuming homogeneous media. At the mesoscale, the medium is heterogeneous and structured, and the availability of transport pathways depends on local morphology.

Definition 5.1 (Admissible Flux)**.** *A transport field $\mathbf{v}(x,t)$ is admissible if it is compatible with the local constraint structure $\Phi(x,t)$, in the sense that motion is permitted only along directions and regions allowed by Φ.*

5.2. Mobility as a Structural Functional

Proposition 5.2 (Structure-Dependent Mobility)**.** *Let $\mu : \mathbb{R} \to \mathbb{R}_{>0}$ be a smooth function. Then the effective transport satisfies $\mathbf{v} \sim -\,\mu(\Phi)\,\nabla\Psi$ for an appropriate driving potential Ψ.*

Remark 5.3. *Regions of low constraint (small Φ) correspond to high mobility, while highly ordered or aggregated regions suppress transport. This captures the empirical observation that conduction and flow are localized to specific pathways within structured media.*

5.3. Emergence of Transport Networks

The spatial variation of Φ induces heterogeneity in $\mu(\Phi)$, leading to the formation of transport networks.

Definition 5.4 (Transport Network)**.** *A transport network is the set $\mathcal{N} = \{x \in \Omega : \mu(\Phi(x)) \text{ is locally maximal}\}$, representing regions where transport is preferentially concentrated.*

These networks correspond to conductive pathways in polymers, fluid channels in gels, and diffusion pathways in porous materials.

5.4. Bidirectional Coupling

Transport not only depends on structure but feeds back into it. This coupling appears explicitly in the variational derivative of the free-energy functional:

$$\frac{\delta \mathcal{F}}{\delta \Phi} \supset \frac{1}{2}\,\mu'(\Phi)\,|\mathbf{v}|^2.$$

High transport activity can induce local reorganization—alignment of polymer chains under shear, restructuring of networks under flow—while the constraint landscape simultaneously modulates where transport occurs. This bidirectionality is the formal expression of the claim that transport shapes structure and structure shapes transport.

5.5. Anisotropic Transport

In many systems, transport is directionally biased by the underlying structure. Introducing a mobility tensor $\mathbf{M}(\Phi)$, the transport law becomes

$$\mathbf{v} = -\,\mathbf{M}(\Phi)\,\nabla\Psi,$$

where the eigenvectors of $\mathbf{M}(\Phi)$ determine preferred directions and the eigenvalues determine relative mobility along those directions.

5.6. Transport and Dissipation

Transport processes are inherently dissipative. The rate of energy dissipation is

$$\mathcal{D} = \int_\Omega \frac{1}{\mu(\Phi)}\,|\mathbf{v}|^2\,dx,$$

which appears as a source term in the evolution of the configurational accessibility field.

Proposition 5.5 (Dissipation Inequality)**.** *For a closed system, $\frac{d}{dt}\mathcal{F} \leq 0$, with equality only at equilibrium.*

5.7. Examples Across Domains

The structural origin of transport is visible across diverse systems. In conjugated polymers, electrical conduction follows percolating pathways defined by morphology [3, 20]. In gels and membranes, ion transport occurs through channels determined by network structure. In emulsions and porous media, fluid flow is confined to interconnected regions of low constraint. In biological systems, molecular transport is regulated by structured environments such as membranes and cytoskeletal networks. In each case, motion is constrained by structure and feeds back into it.

6. Interfaces as Active Boundaries

Interfaces are not passive geometric features of mesoscale systems. They are active constraint surfaces that regulate interaction, aggregation, and transport across the domains they separate. This section formalizes their role within the unified framework.

6.1. Interfaces as Constraint Surfaces

An internal boundary $\Gamma \subset \Omega$ separating two morphological phases represents a region where the structural field Φ transitions sharply between distinct values. Within the diffuse-interface description, Φ varies smoothly across Γ over a width set by ℓ_*. In the sharp-interface limit, Φ is discontinuous across Γ, and the dynamics of the boundary itself become the relevant object.

Definition 6.1 (Active Interface)**.** *An interface Γ is active if it imposes constraints on the admissible configurations and fluxes of $\mathcal{X}$ on both sides, thereby shaping the evolution of Φ, $\mathbf{v}$, and $\mathcal{S}$ in its vicinity.*

Oil–water boundaries in emulsions, lipid bilayer membranes, nanoparticle coatings, and aptamer-functionalized surfaces all fall within this class. Their activity arises not from their static geometry but from the constraints they impose on neighboring field evolution.

6.2. Interface Motion

Taking the sharp-interface limit of the structural evolution equation yields a surface evolution law of the form

$$V_n \;=\; M_\Gamma \left(\kappa\, \mathcal{H} \;-\; [\![f_{\mathrm{loc}}]\!] \;-\; \frac{1}{2}\, [\![\mu'(\Phi)]\!]\, |\mathbf{v}|^2 \right), \tag{3}$$

where V_n is the normal velocity of Γ, $\mathcal{H}$ is its mean curvature, M_Γ is the interface mobility, and $[\![\cdot]\!]$ denotes the jump of a quantity across Γ.

The curvature term $\kappa\mathcal{H}$ drives interface smoothing. The jump in the local free-energy density $[\![f_{\mathrm{loc}}]\!]$ drives motion toward lower-energy configurations. The transport-dependent jump $[\![\mu'(\Phi)]\!]|\mathbf{v}|^2$ can stabilize or destabilize the interface depending on the local flux asymmetry. Equation (3) governs oil–water interfaces, grain boundaries, membrane deformation, and phase boundaries in nanocomposites within a single formalism.

6.3. Interfaces as Transport Regulators

Beyond structural dynamics, interfaces regulate transport. A membrane selects which molecular species cross it; a nanoparticle coating controls surface affinity; an aptamer-functionalized boundary binds specific targets. In each case, the interface imposes asymmetric constraints on $\mathbf{v}$: fluxes that are admissible on one side may be forbidden on the other.

This selectivity is not an additional design feature but a consequence of the structure of the constraint field Φ in the vicinity of Γ. By engineering Φ near an interface—through surfactant chemistry, polymer brush density, or surface functionalization—one engineers the admissible flux, which is to say the transport function of the boundary.

6.4. Interfaces and Configurational Accessibility

Interfaces also shape the local configurational accessibility $\mathcal{S}$. Near a sharp boundary, the range of admissible trajectories is restricted by geometric confinement and interaction asymmetry. The accessibility field is therefore lower near interfaces than in bulk phases, which in turn stabilizes interface position: once an interface forms, the local suppression of $\mathcal{S}$ makes it harder for the boundary to dissolve.

This mechanism explains the observed persistence of mesoscale interfaces under conditions where bulk phases would rapidly equilibrate, and provides a trajectory-accessible account of interfacial stability that does not require invoking long-range forces.

6.5. Examples Across Domains

Emulsion droplets stabilized by nanoparticles or surfactants represent systems where the interface actively controls aggregation and coalescence [10, 14]. Lipid bilayer membranes regulate molecular transport with sub-nanometer selectivity while remaining mechanically deformable. Nanodiscs and lipid-coated nanoparticles present functionalized interfaces that determine binding specificity [16]. Aptamer-modified surfaces bind targets through shape- and charge-complementarity encoded in the interface geometry [15]. Nanoplastic particles interact with biological membranes through interface-mediated constraint modification [19]. In each case, the interface is not a passive boundary but an active organizing element of the mesoscale field.

7. Trajectory-Aware Mesoscale Representation

The preceding sections describe mesoscale matter as a coupled evolution of structure, transport, and configurational accessibility. However, a further representational problem remains. If mesoscale systems evolve through configuration space, then a useful model must preserve not only the state of the system at a given time, but also the trajectory by which that state became available.

This motivates a trajectory-aware description of mesoscale dynamics. A state $\mathcal{X}(x,t)$ should not be treated as an isolated snapshot, nor should its past be compressed into a single hidden variable. Rather, the system should be represented as a collection of overlapping trajectory fragments whose boundaries retain reconstructible information.

7.1. Trajectory Patches

Let $\gamma : [t_0, t_1] \to \mathcal{C}$ denote a trajectory through the configuration space of the system. Instead of representing γ globally, we cover it by local trajectory patches $\{U_i\}_{i\in I}$ with $\gamma([t_0,t_1]) \subseteq \bigcup_{i\in I} U_i$. Each patch U_i contains a local description of the fields $\mathcal{X}_i = (\Phi_i, \mathbf{v}_i, \mathcal{S}_i)$, together with boundary data describing how the trajectory enters and exits that patch. The patch is not merely a compressed state: it is a local history-bearing object that stores

enough information to constrain reconstruction across neighboring patches.

7.2. Overlap Consistency

If two patches overlap, their descriptions must agree on the shared region. For $U_i \cap U_j \neq \varnothing$, we require

$$\rho_{ij}(\mathcal{X}_i) = \rho_{ji}(\mathcal{X}_j) \quad \text{on } U_i \cap U_j,$$

where ρ_{ij} and ρ_{ji} are restriction maps onto the overlap. Memory is preserved by overlap, not by a single global hidden state. Failure of compatibility corresponds to a reconstruction obstruction: the system cannot be consistently reassembled from its local descriptions.

7.3. Non-Markovian Memory Across Scales

For mesoscale systems, the Markovian assumption that the future depends only on the present state is generally too strong. Interfaces, aggregates, polymer networks, and biological assemblies retain path-dependent structure. We therefore introduce a memory functional

$$\mathcal{M}_i(t) = \int_{t-\tau}^{t} K_i(t-s)\, \mathcal{O}_i[\mathcal{X}(s)]\, ds,$$

where K_i is a scale-dependent memory kernel and $\mathcal{O}_i$ is an observable associated with patch U_i. The memory depth τ may vary across scales, allowing fine-scale processes to relax quickly while larger structures preserve longer histories. The evolution equation for the mesoscale field then takes the generalized form

$$\partial_t \mathcal{X}_i = \mathcal{D}_i[\mathcal{X}_i] + \mathcal{G}_i[\mathcal{M}_i] + \eta_i,$$

where $\mathcal{D}_i$ encodes local field dynamics, $\mathcal{G}_i$ encodes memory-dependent correction, and η_i denotes fluctuations.

7.4. Wilson's Façades and the Origin of the Patch Structure

The trajectory-aware tiling developed in this section has a direct conceptual origin in Mark Wilson's analysis of hierarchical scale boundaries in physical theory [27, 28]. Wilson argues, across both *Wandering Significance* and *Physics Avoidance*, that the descriptive vocabulary of classical physics does not extend uniformly across scales. Instead, physical concepts operate locally within patches of validity, and the actual structure of scientific description is a *façade*: a patchwork of locally coherent frameworks whose boundaries are governed by handoff conditions rather than smooth reduction.

Wilson's central observation is that this patchwork structure is not a deficiency of current physics awaiting correction by a future unified theory. It is the operative structure of successful physical description. The seams between patches are not approximations to be eliminated but active boundaries at which different descriptive frameworks must be made mutually consistent. Failure to recognize this—the assumption that a single global vocabulary governs all scales—is what Wilson calls physics avoidance.

The configuration bundle introduced in Section 8 is a direct formalization of this picture. Each patch U_i carries a locally valid field description $\mathcal{X}_i$; the overlap conditions $\rho_{ij}(\mathcal{X}_i) = \rho_{ji}(\mathcal{X}_j)$ are the formal expression of Wilson's handoff conditions; and the gluing functional $\mathcal{C}$ penalizes inconsistency at the seams. The TARTAN framework was developed from this foundation, with the additional observation that mesoscale systems carry non-Markovian memory across scale boundaries—information that a purely instantaneous handoff condition would discard.

Mesoscale systems resist global unified description not because the theory is incomplete, but because the operative physical vocabulary—aggregation, transport, accessibility—is itself scale-local. Each experimental technique accesses one patch of the façade. In this sense, the projection operators Π_k of Section 9 function as localized descriptive frameworks, whose collective action reconstructs the observable structure of the system without requiring a single global representation.

7.5. Reconstruction Pressure

The central difference between trajectory-aware representation and ordinary compression is reconstruction pressure. A model that merely predicts the next state may discard information that is irrelevant to immediate prediction but essential for long-term coherence. A trajectory-aware model penalizes loss of reconstructibility. Let $\widehat{\mathcal{X}}$ denote a field obtained from local patches. The reconstruction loss

$$\mathcal{L}_{\text{rec}} = \sum_i \|\mathcal{X}_i - \widehat{\mathcal{X}}_i\|^2 + \sum_{i,j} \|\rho_{ij}(\mathcal{X}_i) - \rho_{ji}(\mathcal{X}_j)\|^2$$

enforces both local fidelity and overlap consistency. The second term prevents the system from learning locally accurate but globally incompatible representations.

7.6. TARTAN as a Mesoscale Memory Principle

This construction—trajectory-aware recursive tiling of configuration space, with local field information on each tile, boundary compatibility across overlaps, and scale-dependent memory—provides the missing bridge between measurement and dynamics. Experimental techniques project the system into partial observables; trajectory-aware tiling explains how those partial observables can be reintegrated into a coherent history-bearing field. The result is a strengthened form of the central thesis: mesoscale function is not only stabilized dynamics, but stabilized dynamics whose history remains locally reconstructible across scales.

7.7. The Admissibility Log: From Discrete Events to Continuous Fields

The transition between discrete event systems and continuous field dynamics is handled by an admissibility log. Let

$$e_n = (x_n,\, t_n,\, \Delta\Phi_n,\, \Delta\mathbf{v}_n,\, \Delta\mathcal{S}_n)$$

denote a discrete event — a Spherepop operation, local rupture, binding event, acoustic strike, or structural transition. The admissibility log is the ordered collection $\mathcal{L} = \{e_0, e_1, \ldots, e_N\}$ together with compatibility relations specifying which events may follow which others. Each event updates the continuous RSVP field by a localized operator

$$\mathcal{X}_{n+1} = \mathcal{X}_n + \mathcal{U}_{e_n}[\mathcal{X}_n], \qquad \mathcal{X}_n = (\Phi_n, \mathbf{v}_n, \mathcal{S}_n).$$

Discrete events are therefore not external interruptions of the field but localized admissible transformations of it. In the continuum limit, as event spacing tends to zero, the admissibility log induces the field evolution

$$\partial_t \mathcal{X} = \lim_{\Delta t \to 0} \frac{\mathcal{U}_{e_n}[\mathcal{X}]}{\Delta t},$$

recovering the RSVP action-level description. Conversely, coarse-graining a continuous trajectory produces a discrete admissibility log by recording only the events at which the admissible trajectory class changes.

The log therefore mediates between two descriptions:

$$\text{discrete events} \longleftrightarrow \text{admissibility log} \longleftrightarrow \text{RSVP field dynamics.}$$

From the sheaf-theoretic perspective developed in Section 13, the admissibility log is a discrete record of gluing operations: each event records a local change in the section structure, while the full log records whether these local changes can be assembled into a globally coherent trajectory. The log is therefore the finite-event analogue of the Čech cocycle, and its compatibility relations are the discrete analogue of the sheaf gluing condition. Equivalently, the admissibility log presents a composable path in the configuration groupoid, with compatibility relations encoding the descent data required for its realization as a global section.

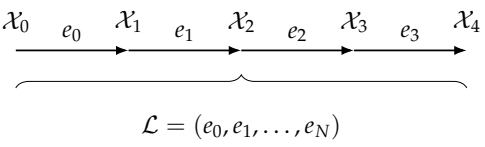

Figure 3: The admissibility log as a composable path in the configuration groupoid: field states as objects, events as 1-morphisms, and the full log as a presentation of trajectory history.

7.8. The Admissibility Log as an ∞-Categorical Object

The admissibility log can be lifted from a sequence of discrete updates to an ∞-categorical structure. Let $\mathcal{C}_{\text{adm}}$ denote the ∞-groupoid of admissible configurations. Objects of $\mathcal{C}_{\text{adm}}$ are field states $\mathcal{X} = (\Phi, \mathbf{v}, \mathcal{S})$. A discrete event $e_n : \mathcal{X}_n \to \mathcal{X}_{n+1}$ is a 1-morphism, represented by the update operator $\mathcal{X}_{n+1} = \mathcal{X}_n + \mathcal{U}_{e_n}[\mathcal{X}_n]$. Composition of events defines paths:

$$e_{n+k} \circ \cdots \circ e_{n+1} \circ e_n : \mathcal{X}_n \to \mathcal{X}_{n+k+1}.$$

The admissibility log $\mathcal{L} = (e_0, e_1, \ldots, e_N)$ therefore presents a composable path in $\mathcal{C}_{\text{adm}}$.

Higher morphisms encode equivalences between event histories. A 2-morphism $\alpha : (e_2 \circ e_1) \Rightarrow (e_2' \circ e_1')$ records that two distinct local event sequences produce equivalent field transformations up to admissible deformation. Higher morphisms encode higher-order compatibility among such equivalences. Trajectory memory is therefore not an auxiliary variable but higher gluing data: non-Markovianity arises when distinct paths with identical endpoints are not equivalent in $\mathcal{C}_{\text{adm}}$, so that two systems may share the same final field state while retaining different admissibility histories.

The TARTAN patch structure supplies descent data for this ∞-groupoid. Each patch U_i carries a local path object $\mathcal{L}_i \in \mathcal{C}_{\text{adm}}(U_i)$, and overlaps require equivalences $\mathcal{L}_i|_{U_i \cap U_j} \simeq \mathcal{L}_j|_{U_i \cap U_j}$. Failure of these equivalences defines a higher obstruction to global reconstruction. Functional lock-in corresponds to collapse to a small subcategory: field states, events as 1-morphisms, equivalent histories as 2-morphisms, memory as higher gluing data, TARTAN consistency as descent, and functional lock-in as confinement to a restricted subcategory.

7.9. Variational Origin of the Event Operator

Each discrete event e_n may be derived from a time-discretized variational principle, grounding the admissibility-log update physically. Let the continuous RSVP action be

$$\mathcal{A}[\mathcal{X}] = \int_{t_n}^{t_{n+1}} L(\mathcal{X}, \partial_t \mathcal{X}, \nabla \mathcal{X})\, dt.$$

Discretizing over a time step Δt gives

$$\mathcal{A}_n = \Delta t\, L\left(\mathcal{X}_n, \frac{\mathcal{X}_{n+1} - \mathcal{X}_n}{\Delta t}, \nabla \mathcal{X}_n\right).$$

The event operator $\mathcal{U}_{e_n}$ is defined by the variational update $\mathcal{X}_{n+1} = \mathcal{X}_n + \mathcal{U}_{e_n}[\mathcal{X}_n]$, where $\mathcal{U}_{e_n}$ is chosen so that $\delta \mathcal{A}_n = 0$ subject to admissibility constraints. An event is therefore not arbitrary but a localized extremal update of the RSVP action. In the limit $\Delta t \to 0$, the admissibility log recovers the continuous field equations; at finite resolution, it records the discrete operators by which the field evolves.

Proposition 7.1 (Continuum Limit of the Admissibility Log)**.** *Let $\{\mathcal{L}_{\Delta t}\}$ be a family of admissibility logs with event spacing $\Delta t \to 0$, where each event operator $\mathcal{U}_{e_n}$ is derived from the discrete action $\mathcal{A}_n$ and satisfies a uniform Lipschitz bound $\|\mathcal{U}_{e_n}[\mathcal{X}] - \mathcal{U}_{e_n}[\mathcal{X}']\| \leq L\|\mathcal{X} - \mathcal{X}'\|$. Then the piecewise-linear interpolation of $\mathcal{X}_n$ converges, in L^2_{loc} or a suitable Sobolev space, to a weak solution of the continuous RSVP evolution equation $\partial_t \mathcal{X} = \mathcal{D}[\mathcal{X}]$, where $\mathcal{D}$ is the variational derivative induced by the continuous action.*

Sketch. The discrete updates define a forward Euler scheme for the variational flow. Uniform Lipschitz continuity ensures stability, while bounded energy decrease provides compactness. Standard arguments for convergence of minimizing movements or gradient flows then yield convergence to a weak solution. □

7.10. Events as Tokens in Embedding Space

The admissibility log admits a parallel computational interpretation. Each event $e_n = (x_n, t_n, \Delta\Phi_n, \Delta\mathbf{v}_n, \Delta\mathcal{S}_n)$ may be mapped into an embedding vector $z_n = E(e_n) \in \mathbb{R}^d$, so the log becomes a trajectory in embedding space $\mathcal{L} = (z_0, z_1, \ldots, z_N)$. Compatibility between events is represented by transition constraints $C(z_n, z_{n+1}) \geq 0$, determining whether one event may admissibly follow another. In this interpretation, TARTAN supplies the patch structure, CLIO supplies the repair operator when compatibility fails, and the embedding trajectory supplies the computational analogue of RSVP field evolution. A failed transition $C(z_n, z_{n+1}) < 0$ corresponds to a gluing obstruction, while a successful repair $z'_{n+1} = \text{CLIO}(z_n, z_{n+1})$ with $C(z_n, z'_{n+1}) \geq 0$ corresponds to local section correction. The admissibility log therefore has two readings: in physics, it discretizes an action; in cognition, it records a trajectory of constrained symbolic-semantic updates. In both cases, coherence means that local transitions can be glued into a global trajectory.

8. Toward a Unified Framework: Constrained Field Dynamics

The preceding analysis establishes three complementary views of mesoscale systems: a variational description of structure via Φ, a transport description via $\mathbf{v}$ constrained by Φ, and a trajectory-aware representation in which dynamics are encoded by overlapping patches with non-Markovian memory. We now synthesize these into a single mathematical framework.

8.1. State Space and Configuration Bundle

We retain the mesoscale state $\mathcal{X}(x,t) = \big(\Phi(x,t),\ \mathbf{v}(x,t),\ \mathcal{S}(x,t)\big)$ on $\Omega \subset \mathbb{R}^d$. To incorporate trajectory-aware structure, we augment this with a covering $\{U_i\}_{i \in I}$ of spacetime $\Omega \times [0,T]$ and define local fields $\mathcal{X}_i = \mathcal{X}|_{U_i}$.

Definition 8.1 (Mesoscale Configuration Bundle)**.** *The collection $\{\mathcal{X}_i\}_{i \in I}$ together with restriction maps $\rho_{ij} : \mathcal{X}_i \to \mathcal{X}_j$ on overlaps $U_i \cap U_j$ defines a configuration bundle over spacetime.*

Consistency across overlaps imposes gluing conditions $\rho_{ij}(\mathcal{X}_i) = \rho_{ji}(\mathcal{X}_j)$, ensuring that local descriptions assemble into a coherent global field.

8.2. Free-Energy Functional

The free-energy functional governs equilibrium and near-equilibrium behavior:

$$\mathcal{F}[\mathcal{X}] = \int_\Omega \Big[f_{\text{loc}}(\Phi) + \tfrac{\kappa}{2}|\nabla\Phi|^2 + \tfrac{1}{2}\mu(\Phi)|\mathbf{v}|^2 - \lambda\,\mathcal{S} \Big] dx + \sum_i \int_{U_i} \mathcal{G}_i[\mathcal{M}_i]\, dx\, dt, \tag{4}$$

where $f_{\text{loc}}(\Phi)$ is a local bulk free-energy density encoding thermodynamics of the order parameter, $\kappa > 0$ is an interfacial stiffness, $\mu(\Phi)$ is a structure-dependent mobility coupling transport to the structural state, and $\lambda > 0$ is an accessibility weight. The term $-\lambda\mathcal{S}$ promotes exploration of configurations with high accessibility, reflecting the tendency of the system to occupy regions of configuration space with many admissible trajectories. In contrast, the dynamical term $-\beta(\Phi)\mathcal{S}$ in equation (7) encodes the irreversible collapse of accessibility induced by increasing constraint. The resulting competition between exploration and collapse governs the transient accessibility landscape and determines which regions of configuration space remain dynamically reachable. The memory term $\mathcal{G}_i[\mathcal{M}_i]$ encodes the contribution of trajectory coherence across scales.

8.3. Dissipative Dynamics with Memory Coupling

The evolution equations generalize local dynamics by including memory contributions.

For the structural field:

$$\partial_t \Phi = \nabla \cdot \left(M(\Phi)\, \nabla \frac{\delta \mathcal{F}}{\delta \Phi} \right) + \mathcal{K}_\Phi[\mathcal{M}] + \eta_\Phi, \tag{5}$$

where the variational derivative expands as

$$\frac{\delta \mathcal{F}}{\delta \Phi} = f'_{\text{loc}}(\Phi) - \kappa\,\Delta\Phi + \tfrac{1}{2}\mu'(\Phi)|\mathbf{v}|^2,$$

so that transport activity feeds back explicitly into structural evolution through the term $\mu'(\Phi)|\mathbf{v}|^2$.

For the transport field:

$$\partial_t \mathbf{v} = -\frac{1}{\mu(\Phi)}\mathbf{v} - \nabla p + \nabla \cdot \sigma(\Phi, \mathbf{v}) + \mathcal{K}_{\mathbf{v}}[\mathcal{M}] + \eta_{\mathbf{v}}. \tag{6}$$

The prefactor $\mu(\Phi)^{-1}$ suppresses motion in highly ordered, low-mobility regions, implementing the structural origin of anisotropic and heterogeneous transport.

For the configurational accessibility field:

$$\partial_t \mathcal{S} = \underbrace{\alpha_\Phi \left| \nabla \tfrac{\delta \mathcal{F}}{\delta \Phi} \right|^2}_{\text{structural exploration}} + \underbrace{\alpha_v\, |\mathbf{v}|^2}_{\text{transport diversif.}} - \underbrace{\beta(\Phi)\,\mathcal{S}}_{\text{constraint collapse}} - \nabla \cdot \mathbf{J}_\mathcal{S} + \mathcal{K}_\mathcal{S}[\mathcal{M}], \tag{7}$$

where $\alpha_\Phi, \alpha_v > 0$ and $\beta(\Phi) > 0$ with $\beta'(\Phi) > 0$. The monotonic dependence of β on Φ encodes constraint-induced collapse: increasingly ordered regions suppress local configurational accessibility faster, producing the positive feedback loop

$$\Phi \uparrow \Rightarrow\ \beta(\Phi) \uparrow \Rightarrow\ \mathcal{S} \downarrow$$

$$\Rightarrow \text{ fewer escape trajectories } \Rightarrow\ \Phi \uparrow .$$

This loop is the dynamical signature of gelation, crystallization, fiber bundling, and biological folding lock-in: processes in which a system progressively forecloses its own future options as it orders. In particular, regions that transiently increase in Φ experience accelerated accessibility collapse, making such fluctuations self-reinforcing and driving the system toward locally irreversible organization. This mechanism provides a unified dynamical account of structuring processes in which order stabilizes itself by eliminating alternative trajectories.

8.4. Gluing Constraints as Dynamical Conditions

The overlap consistency conditions introduce additional dynamical terms through the gluing functional

$$\mathcal{C} = \sum_{i,j} \int_{U_i \cap U_j} \|\rho_{ij}(\mathcal{X}_i) - \rho_{ji}(\mathcal{X}_j)\|^2\, dx\, dt,$$

which penalizes inconsistency across patches.

Proposition 8.2 (Gluing-Driven Regularization)**.** *Including $\mathcal{C}$ in the effective action introduces forces that drive the system toward cross-scale coherence.*

8.5. Equilibrium and Metastable States

Equilibrium configurations correspond to minimizers of the total functional $\mathcal{F}_{\text{tot}} = \mathcal{F} + \mathcal{C}$. Metastable states arise as local minima, with transitions between them mediated by configurational accessibility and memory effects.

Remark 8.3. *The presence of memory terms modifies the effective energy landscape, introducing path-dependent stability and hysteresis.*

8.6. Variational Characterization of Stable Morphologies

For a system conserving total order-parameter content $\int_\Omega \Phi\, dx = \bar{\Phi}$, the equilibrium problem is

$$\min_{\Phi} \ \mathcal{F}[\Phi] \quad \text{subject to} \quad \int_\Omega \Phi\, dx = \bar{\Phi},$$

with Euler–Lagrange equation

$$f'_{\mathrm{loc}}(\Phi) - \kappa\, \Delta\Phi = \mu_0,$$

where μ_0 is a Lagrange multiplier fixed by the constraint. The solutions are precisely the self-assembled morphologies observed across domains: microphase- separated patterns, lamellae, cylinders, and bicontinuous networks emerge as different solution branches depending on $\bar{\Phi}$, κ, and the shape of f_{loc}.

8.7. Functional Regime

Definition 8.4 (Functional Regime)**.** *A functional regime is a subset of configuration space in which trajectories of $\mathcal{X}$ are stable under perturbations, satisfy gluing consistency across all relevant scales, and are confined to regions where $\mathcal{S}$ is persistently low.*

Functional systems correspond to trajectories that enter and remain within low-$\mathcal{S}$ regions of configuration space, where configurational accessibility has been suppressed and dynamics become reproducible. This formalizes the earlier proposition and makes explicit what it means for a system to be functional: it has foreclosed enough futures that its evolution is predictable.

8.8. Dimensional Reduction and Observables

Different experimental techniques probe different aspects of $\mathcal{X}$, each corresponding to a projection operator $\Pi_k : \mathcal{X} \mapsto Y_k$. Scattering measures spatial correlations $\hat{\Phi}(q)^2$; rheology accesses the linear response of $\mathbf{v}$ to applied stress; spectroscopy probes transition rates encoding the structure of $\mathcal{S}$ near saddle points of $\mathcal{F}$; imaging provides localized samples of $\Phi(x, t_0)$ at fixed time. Each is a linearly independent projection of the same object, which explains why they are consistent without being redundant. The present framework provides the forward model against which reconstructions from these projections are calibrated.

9. Well-Posedness, Stability, and Regularity

The evolution equations governing $\mathcal{X}(x,t) = (\Phi, \mathbf{v}, \mathcal{S})$ have been introduced in variational and geometric form. We now establish that they define a well-posed dissipative dynamical system, elevating the framework from a structural description to a rigorous PDE theory.

9.1. Functional Setting and Admissible State Space

Let $\Omega \subset \mathbb{R}^d$ be a bounded domain with sufficiently regular boundary $\partial\Omega$, and let $[0, T]$ be a finite time horizon. Define the admissible state space

$$\mathcal{X} := H^1(\Omega) \times L^2(\Omega)^d \times L^2(\Omega),$$

where $\Phi \in H^1(\Omega)$ is the structural constraint field, $\mathbf{v} \in L^2(\Omega)^d$ is the transport field, and $\mathcal{S} \in L^2(\Omega)$ is the configurational accessibility field. Initial data $\mathcal{X}_0 = (\Phi_0, \mathbf{v}_0, \mathcal{S}_0) \in \mathcal{X}$ is prescribed together with appropriate boundary conditions (Dirichlet, Neumann, or periodic depending on the domain geometry).

9.2. Assumptions on Coefficients

To establish well-posedness we impose the following conditions. The mobility and dissipation coefficients satisfy $M(\Phi), \mu(\Phi) \in C^1(\mathbb{R})$ with $M(\Phi), \mu(\Phi) \geq c_0 > 0$. The free-energy density satisfies $f_{\mathrm{loc}} \in C^2(\mathbb{R})$ with $|f''_{\mathrm{loc}}(\Phi)| \leq C(1 + |\Phi|^p)$ for some $p \geq 1$. The collapse function satisfies $\beta(\Phi) \in C^1(\mathbb{R})$, $\beta \geq 0$, and $\beta' \geq 0$. Memory kernels satisfy $K_i \in L^1([0, T])$, and forcing terms satisfy $\eta \in L^2([0, T]; \mathcal{X})$.

9.3. Energy Dissipation and Lyapunov Structure

Define the total Lyapunov functional

$$\mathcal{L}[\mathcal{X}] = \mathcal{F}[\mathcal{X}] + \lambda \int_\Omega \mathcal{S}(x)\, dx.$$

Proposition 9.1 (Dissipation Inequality)**.** *Under the assumptions above, weak solutions satisfy*

$$\frac{d}{dt}\mathcal{L}[\mathcal{X}(t)] \leq -\int_\Omega \Big(M(\Phi) \big| \nabla \tfrac{\delta \mathcal{F}}{\delta \Phi} \big|^2 + \tfrac{|\mathbf{v}|^2}{\mu(\Phi)} + \beta(\Phi)\mathcal{S} \Big)\, dx + \mathcal{R}(t),$$

where $\mathcal{R}(t)$ is bounded in $L^1([0, T])$.

The dissipation is structural: constraint gradients, transport, and accessibility all decay unless

sustained by external forcing or memory. The term $\beta(\Phi)\mathcal{S}$ enforces accessibility collapse in high-constraint regions, providing the dynamical mechanism for functional lock-in.

9.4. Existence of Weak Solutions

Theorem 9.2 (Existence of Weak Solutions)**.** *Let $\mathcal{X}_0 \in \mathcal{X}$. Under the assumptions of the preceding subsection, there exists a weak solution*

$$\mathcal{X} \in L^2(0,T;\mathcal{X}), \qquad \partial_t \mathcal{X} \in L^2(0,T;\mathcal{X}^*)$$

satisfying the RSVP evolution equations in the distributional sense.

Sketch. Construct a Galerkin approximation in finite-dimensional subspaces. The dissipation inequality provides uniform energy bounds. Apply the Aubin–Lions compactness lemma to extract a convergent subsequence. Pass to the limit in nonlinear terms using weak continuity. Memory terms remain controlled by the L^1 boundedness of kernels. □

9.5. Stability of Functional Regimes

Proposition 9.3 (Stability of Low-$\mathcal{S}$ Regimes)**.** *If $\beta(\Phi)$ is uniformly bounded below and strictly positive on U, then perturbations of a functional equilibrium $\mathcal{X}^*$ decay exponentially:*

$$\|\mathcal{X}(t) - \mathcal{X}^*(t)\|_{\mathcal{X}} \leq Ce^{-\gamma t}.$$

Functional systems therefore correspond to dynamically stable attractors characterized by suppressed configurational accessibility. Higher regularity of solutions depends on coefficient smoothness; sharp interfaces arise as controlled singularities of Φ rather than breakdown of the solution itself.

9.6. Discrete-to-Continuum Convergence

Proposition 9.4 (Admissibility Log Convergence)**.** *Let $\mathcal{X}_{\Delta t}(t)$ denote the piecewise-linear interpolation of states generated by admissibility-log updates with timestep Δt. Under Lipschitz continuity of update operators and bounded energy dissipation, $\mathcal{X}_{\Delta t} \to \mathcal{X}$ in $L^2(0,T;\mathcal{X})$ as $\Delta t \to 0$.*

This establishes that the admissibility log defines a consistent discretization of the continuous RSVP dynamics, grounding the computational framework in rigorous PDE theory.

10. Equivalence Theorem: Accessibility, Cohomology, and Homotopy

The RSVP framework admits multiple formal characterizations of functional structure: dynamical (low $\mathcal{S}$), sheaf-theoretic (vanishing gluing obstruction), and topological (reduction in admissible homotopy classes). We now prove that these are equivalent descriptions of the same underlying constraint regime.

10.1. Definitions

Let $\mathcal{X}$ be a weak solution on $\Omega \times [0,T]$, and let $\{U_i\}$ be an open cover. The configurational accessibility is $\mathcal{S}(x,t) = \log \mathrm{Vol}(\mathcal{P}_{x,t})$, the Čech obstruction is $\delta_{ij} = \mathcal{X}_i|_{U_i \cap U_j} - \mathcal{X}_j|_{U_i \cap U_j}$, the obstruction functional is

$$\mathcal{O}[\mathcal{X}] = \sum_{i,j} \int_{U_i \cap U_j} \|\delta_{ij}\|^2 \, dx\, dt,$$

and $\pi_0(\mathcal{P}_{x,t})$ denotes the set of admissible homotopy classes of trajectories through (x,t).

10.2. Equivalence Theorem

Theorem 10.1 (RSVP Equivalence Principle)**.** *Under the regularity and coercivity conditions of the well-posedness section, the following are equivalent on any bounded region $U \subset \Omega$:*

1. (Accessibility collapse) $\mathcal{S}(x,t) \leq \varepsilon$ *for all* $x \in U$, $t \in [t_0, t_1]$.
2. (Cohomological triviality) $\mathcal{O}[\mathcal{X}] = 0$, *equivalently* $[\delta] = 0 \in \check{H}^1(\{U_i\}, \mathcal{F})$.
3. (Homotopy collapse) $|\pi_0(\mathcal{P}_{x,t})| \leq N < \infty$.
4. (Dynamical stability) $\|\mathcal{X}(t) - \mathcal{X}^*(t)\|_{\mathcal{X}} \leq Ce^{-\gamma t}$ *for some equilibrium* $\mathcal{X}^*$.

Sketch. $(1 \Rightarrow 3)$: Bounded $\mathcal{S}$ implies bounded trajectory volume, restricting the number of admissible homotopy classes.

$(3 \Rightarrow 2)$: Finitely many trajectory classes force local sections to agree on overlaps, eliminating nontrivial cocycles.

$(2 \Rightarrow 4)$: Vanishing obstruction ensures global coherence; combined with the dissipation inequality, this yields exponential stability via the Lyapunov functional $\mathcal{L}$.

$(4 \Rightarrow 1)$: Exponential stability contracts trajectory neighborhoods, reducing accessible future states and thereby $\mathcal{S}$. □

Remark 10.2. *This theorem unifies the entropy-like collapse of $\mathcal{S}$, topological reduction of homotopy classes, categorical sheaf consistency, and dynamical stability into a single formal equivalence. They are not separate phenomena but equivalent invariants of functional structure.*

11. Stress–Energy Tensor and General Relativistic Coupling

To embed RSVP within relativistic physics we derive the stress–energy tensor variationally and show its coupling to spacetime curvature through the Einstein field equations.

11.1. Lagrangian Formulation

On a Lorentzian manifold $(\mathcal{M}, g_{\mu\nu})$, define the RSVP Lagrangian density

$$\mathcal{L}_{\text{RSVP}} = f_{\text{loc}}(\Phi) + \tfrac{\kappa}{2}\nabla_\mu\Phi\nabla^\mu\Phi + \tfrac{1}{2}\mu(\Phi)\, g_{\mu\nu}v^\mu v^\nu - \lambda\mathcal{S} + \mathcal{L}_{\mathcal{S}},$$

where $\mathcal{L}_{\mathcal{S}}$ encodes the kinetic and dissipative terms for the accessibility field.

11.2. Stress–Energy Tensor

By the variational definition $T^{\mu\nu} = (2/\sqrt{-g})\,\delta(\sqrt{-g}\,\mathcal{L})/\delta g_{\mu\nu}$, we obtain

$$T^{\mu\nu} = \kappa\nabla^\mu\Phi\nabla^\nu\Phi - g^{\mu\nu}\left(\tfrac{\kappa}{2}\nabla_\alpha\Phi\nabla^\alpha\Phi + f_{\text{loc}}(\Phi)\right) + \mu(\Phi)v^\mu v^\nu - \tfrac{1}{2}g^{\mu\nu}\mu(\Phi)v_\alpha v^\alpha + T_{\mathcal{S}}^{\mu\nu},$$

where $T_{\mathcal{S}}^{\mu\nu}$ encodes accessibility pressure and dissipation. The three contributions have clear interpretations: Φ acts as a coherence-density field sourcing curvature, $\mathbf{v}$ contributes momentum flux, and $\mathcal{S}$ contributes an entropy-like pressure.

11.3. Einstein Field Equations

Coupling to gravity gives

$$G^{\mu\nu} = 8\pi G\, T^{\mu\nu}.$$

In the weak-field limit $g_{\mu\nu} = \eta_{\mu\nu} + h_{\mu\nu}$ with $h_{\mu\nu} = a\Phi\eta_{\mu\nu} + b\partial_\mu\Phi\partial_\nu\Phi + c\nabla_\mu\nabla_\nu\Phi$, variation of the total action $\mathcal{A} = \int[(R/16\pi G) + \mathcal{L}_{\text{RSVP}} + \mathcal{L}_{\text{matter}}]\sqrt{-g}\,d^4x$ with respect to $g_{\mu\nu}$ recovers the previously stated field equations, now derived rather than postulated.

11.4. Geodesics and Curvature from Constraint

Particle trajectories follow geodesics of the effective metric:

$$\frac{d^2x^\mu}{d\tau^2} + \Gamma^\mu_{\alpha\beta}\frac{dx^\alpha}{d\tau}\frac{dx^\beta}{d\tau} = 0.$$

The Christoffel symbols $\Gamma^\mu_{\alpha\beta}$ depend on $h_{\mu\nu}[\Phi, \nabla\Phi, \mathcal{S}]$, so curvature arises from constraint gradients rather than solely from matter density. In the flat limit $\Phi = \text{const}$, $h_{\mu\nu} \to 0$ and special relativity is recovered.

12. Numerical Discretization and Simulation Scheme

We construct a stable numerical scheme consistent with the variational and dissipative structure of RSVP, deriving update rules and stability conditions directly from the PDE theory of the well-posedness section.

12.1. Spatial Discretization

Discretize Ω into a uniform grid with spacing Δx. Define grid fields Φ_i^n, $\mathbf{v}_i^n$, $\mathcal{S}_i^n$. Approximate gradients and Laplacians by centered finite differences:

$$\nabla\Phi \approx \frac{\Phi_{i+1} - \Phi_{i-1}}{2\Delta x}, \qquad \Delta\Phi \approx \frac{\Phi_{i+1} - 2\Phi_i + \Phi_{i-1}}{(\Delta x)^2}.$$

12.2. Semi-Implicit Time Integration

Use semi-implicit stepping, treating diffusive terms implicitly and nonlinear terms explicitly. For the structural field:

$$\Phi^{n+1} = \Phi^n + \Delta t\,\nabla\cdot\left(M(\Phi^n)\nabla\frac{\delta\mathcal{F}}{\delta\Phi^{n+1}}\right).$$

For the transport field:

$$\mathbf{v}^{n+1} = \mathbf{v}^n - \Delta t\left(\frac{1}{\mu(\Phi^n)}\mathbf{v}^n + \nabla p\right).$$

For the accessibility field:

$$\mathcal{S}^{n+1} = \mathcal{S}^n + \Delta t\left(\alpha_\Phi\left|\nabla\tfrac{\delta\mathcal{F}}{\delta\Phi}\right|^2 + \alpha_v|\mathbf{v}|^2 - \beta(\Phi)\mathcal{S}\right).$$

12.3. Stability Condition

The CFL-type stability condition derived from the diffusion terms is

$$\Delta t \le \frac{(\Delta x)^2}{2\max M(\Phi)}.$$

12.4. Discrete Energy Consistency

Proposition 12.1 (Discrete Dissipation)**.** *The semi-implicit scheme satisfies $\mathcal{F}[\mathcal{X}^{n+1}] \leq \mathcal{F}[\mathcal{X}^n]$ under the CFL condition, preserving the dissipative structure of the continuous system.*

12.5. Memory Implementation

Memory kernels are discretized as $\mathcal{M}_i^n = \sum_{k=0}^{n} K(n-k)\,\mathcal{O}_i^k\,\Delta t$. For exponential kernels $K(t) = e^{-\lambda t}$, the recursion $\mathcal{M}^{n+1} = e^{-\lambda \Delta t}\mathcal{M}^n + \mathcal{O}^n$ reduces memory updates to $\mathcal{O}(1)$ per step. This scheme preserves the dissipative structure, constraint–transport coupling, and accessibility collapse dynamics, providing a direct computational realization of RSVP as a trajectory-aware field simulator.

13. A Homotopy-Theoretic Interpretation of Mesoscale Dynamics

The trajectory-aware formulation developed in the preceding sections suggests that mesoscale dynamics are not fully characterized by instantaneous field values, but by the classes of trajectories through configuration space that remain dynamically admissible. This naturally invites a homotopy-theoretic interpretation.

13.1. Trajectories as Paths in Configuration Space

Let $\mathcal{C}$ denote the space of admissible coarse-grained configurations of the system. A trajectory $\gamma : [0, T] \to \mathcal{C}$ corresponds to a path through this space, generated by the evolution of the coupled field $\mathcal{X}(x, t)$. Two trajectories γ_0 and γ_1 are said to be homotopic if one can be continuously deformed into the other through a family of admissible trajectories that remain within $\mathcal{C}$. The admissibility constraint is crucial: deformations that pass through energetically forbidden or dynamically inaccessible configurations are not permitted.

13.2. Configurational Accessibility as Homotopy Volume

Within this interpretation, the configurational accessibility field $\mathcal{S}$ acquires a geometric meaning. Rather than representing thermodynamic entropy, $\mathcal{S}(x, t)$ measures the local volume of admissible homotopy classes of trajectories passing through a given region of configuration space. High $\mathcal{S}$ corresponds to regions where many distinct trajectory classes remain accessible, while low $\mathcal{S}$ corresponds to regions where the system has collapsed onto a small number of homotopy classes.

Interpretation. Accessibility collapse is therefore a homotopy collapse: the progressive elimination of admissible deformations between trajectories.

13.3. Constraint-Induced Homotopy Reduction

The state-dependent collapse term $-\beta(\Phi)\mathcal{S}$ introduced in equation (7) can be interpreted as a reduction in the number of available homotopy classes as structural constraint increases. As Φ increases, admissible deformations between trajectories are restricted. Paths that were previously deformable into one another become separated by constraint barriers, and the configuration space fragments into distinct components that are no longer mutually accessible.

Proposition 13.1 (Homotopy Reduction Under Constraint)**.** *Increasing structural constraint Φ reduces the number of admissible homotopy classes of trajectories, effectively partitioning configuration space into dynamically disconnected regions.*

13.4. Interfaces as Homotopy Boundaries

Interfaces play a distinguished role in this picture. A boundary Γ between phases corresponds to a region where admissibility conditions change discontinuously. Trajectories that cross Γ may not be continuously deformable into trajectories that remain within a single phase. Interfaces therefore do not merely separate regions of space, but separate regions of trajectory space, acting as boundaries between homotopy classes.

13.5. Trajectory Classes and Functional Stability

A functional system is one in which the admissible trajectories are confined to a small number of homotopy classes, and small perturbations do not induce transitions between these classes. Functional regimes therefore correspond to regions where the system has undergone homotopy collapse: many possible evolutions have been eliminated, leaving a restricted set of stable trajectory classes. The patch-based representation introduced in Section 8 models this structure locally. Each patch encodes a local segment of trajectory together with boundary data determining how it can be deformed and glued to neighboring patches. Failure of gluing

corresponds to a homotopy obstruction: the inability to consistently deform local trajectory segments into a global trajectory.

Proposition 13.2 (Accessibility–Homotopy Correspondence)**.** *Let $\pi_0(\mathcal{P}_{x,t})$ denote the set of admissible homotopy classes of trajectories through (x,t). Then there exists a monotone functional relationship*

$$\mathcal{S}(x,t) \;\sim\; \log|\pi_0(\mathcal{P}_{x,t})| + \textit{intra-class volume},$$

so that accessibility collapse implies reduction in the number of homotopy classes, up to measure-zero degeneracy.

This turns the earlier intuition into a structural statement: accessibility collapse is topological collapse, not merely a decrease in trajectory volume.

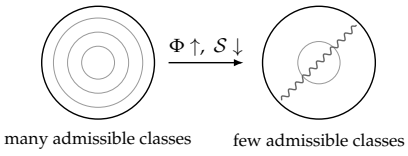

Figure 4: Accessibility collapse reduces both trajectory volume and the number of admissible homotopy classes, the dual signature of functional lock-in.

14. Geometric Unification Across Domains

The preceding development has focused on mesoscale systems in physical and biological contexts. However, the underlying structure of the framework is not specific to these domains. A closely related geometric pattern appears across machine learning, high-dimensional geometry, and quantum modeling. Making this connection explicit clarifies that the constrained-field formulation is a particular instance of a broader class of systems governed by constrained dynamics in high-dimensional spaces.

14.1. High-Dimensional Geometry and Constraint

In high-dimensional geometry, objects are naturally described not by their visual shape but by the constraints that define them. A key feature of high-dimensional spaces is the concentration of measure: volume tends to concentrate in specific regions determined by constraints, so that the behavior of systems is governed less by global geometry than by the structure of admissible directions at each point. This perspective aligns directly with the role of Φ and $\mathcal{S}$ in the present framework. The structural field defines local constraint geometry, while the accessibility field measures the effective volume of admissible directions available for evolution.

14.2. Local Charts and Global Reconstruction

Visualization methods for high-dimensional data rely on constructing local neighborhoods and stitching them together to infer global structure. Nearest- neighbor graphs, manifold learning techniques, and related methods implicitly treat the space as covered by overlapping local charts. This construction is formally analogous to the trajectory-aware tiling introduced in Section 8. Each local chart corresponds to a patch carrying partial information about the system, while consistency across overlaps ensures that local descriptions assemble into a coherent global object. The requirement is the same in both settings: local representations must agree on shared regions, or the global structure cannot be reconstructed.

14.3. Dynamic Geometry in Self-Attention

Transformer architectures extend this geometric picture by introducing dynamics into the representation itself. In self-attention mechanisms, the relative position of elements is not fixed but evolves as a function of context. The system therefore does not operate within a single static geometry, but within a family of context-dependent geometries, and the evolution of representation is trajectory-like: meaning is encoded not only in position, but in the path taken through a sequence of relational transformations. This mirrors the trajectory-aware formulation of mesoscale systems, where $\mathbf{v}$ encodes directed motion through configuration space while the patch-based representation preserves the history of that motion across overlapping regions.

14.4. Quantum Systems and Possibility Space

Quantum systems provide a further example of dynamics governed by constrained exploration of a high-dimensional space. A superposed state corresponds to a high-accessibility regime in which multiple outcomes remain possible. Measurement corresponds to a reduction in accessibility, collapsing the system into a restricted set of states. While the formal structure differs from the classical field description used here, the underlying pattern is the same: systems evolve by exploring a space

of possibilities subject to constraints that progressively restrict that space.

14.5. Unified Interpretation

Across these domains, a common structure emerges. Systems are best understood as evolving within high-dimensional spaces, where constraints define admissible regions and dynamics determine trajectories through those regions. The coupled field $\mathcal{X}(x,t) = (\Phi, \mathbf{v}, \mathcal{S})$ is a specific realization of this principle: systems evolve by progressively restricting the set of admissible trajectories through geometric and dynamical constraints. This interpretation unifies the behavior of mesoscale matter with phenomena observed in machine learning, data representation, and quantum systems, and situates the present framework within a broader geometric understanding of complex systems.

15. Accessibility, Novelty, and Structured Discovery

The preceding sections have developed a physical and geometric account of mesoscale systems in terms of constrained field dynamics. The same structural principles appear in cognitive, perceptual, and creative systems. In particular, the configurational accessibility field $\mathcal{S}$ provides a natural bridge between physical dynamics and processes of discovery and learning.

15.1. Novelty as Accessibility Gradient

A recurring idea in theories of intrinsic motivation is that systems are driven to discover patterns that improve their internal representations. Within the present framework, novelty corresponds to motion through regions of configuration space where $\mathcal{S}$ changes rapidly. Regions of high $\mathcal{S}$ admit many possible continuations but lack structure, while regions of very low $\mathcal{S}$ are overly constrained and predictable. The most informative regimes lie between these extremes, where constraint is emerging but not yet complete.

Remark 15.1. *Aesthetic or epistemic novelty may be interpreted as traversal of regions where $\nabla\mathcal{S}$ is large: the system reduces uncertainty locally while retaining sufficient accessibility to permit further refinement.*

15.2. The Limits of Fixed Objective Functions

Many formal approaches to complex systems emphasize optimization with respect to predefined metrics, implicitly assuming that the relevant structure of the system is already known and that the space of admissible outcomes can be fully specified in advance. In the present framework, this corresponds to fixing a global functional and treating the system as evolving toward its minimizer. However, in many mesoscale and cognitive systems, the admissible configuration space itself evolves with the system: $\mathcal{S}$ changes as constraints emerge, altering which trajectories remain possible. Overreliance on predefined objective functions corresponds to prematurely collapsing $\mathcal{S}$, eliminating trajectories that may be necessary for discovering relevant structure.

15.3. Compression as Structured Reduction

It has been proposed that systems are driven to discover regularities that allow more efficient internal representation, with progress corresponding to increased compressibility of observations [25, 26]. Within the present framework, compression can be interpreted as a reduction in configurational accessibility: a system that identifies a regularity effectively restricts the set of admissible continuations of its internal state. What was previously a large set of possible trajectories becomes a smaller, more constrained set consistent with the discovered pattern.

Reinterpreted geometrically, the drive toward compression corresponds to motion through regions of configuration space where $\mathcal{S}$ decreases in a structured manner. The system is not driven toward minimal accessibility immediately, but toward regions where accessibility can be reduced through the discovery of organization.

Proposition 15.2 (Novelty as Accessibility Descent)**.** *A trajectory is informative if it induces a locally significant decrease in $\mathcal{S}$ while preserving sufficient accessibility for continued evolution.*

This distinguishes meaningful novelty from randomness. Random fluctuations may explore high-$\mathcal{S}$ regions but do not produce sustained reduction. Structured discovery produces persistent constraint, leading to stable regions of low accessibility. Effective learning and creative processes therefore operate near the boundary between exploration and collapse, where accessibility can be reduced incrementally without eliminating the possibility of further discovery.

15.4. Compression as Homotopy Collapse

The interpretation of novelty as structured accessibility reduction admits a direct topological refinement. Compression can be understood not merely as a reduction in the volume of accessible configurations, but as a reduction in the number of admissible homotopy classes. When a system discovers a regularity, it eliminates entire families of trajectories that are no longer consistent with the learned structure.

Proposition 15.3 (Compression as Homotopy Reduction)**.** *Structured compression corresponds to a decrease in the number of admissible homotopy classes of trajectories in configuration space. A compression event imposes additional constraints on admissibility, restricting the allowable trajectories; since homotopy classes are defined relative to admissible deformations, restricting admissibility eliminates entire equivalence classes rather than individual paths.*

This sharpens the distinction between randomness and structure. Random exploration may traverse many trajectories within a given homotopy class but does not change the class itself. Structured discovery alters the topology of the admissible space by removing or separating classes of trajectories. A system is functional when its dynamics are confined to a restricted set of homotopy classes and perturbations do not induce transitions between them. Compression reduces accessibility; accessibility collapse reduces homotopy classes; confinement of homotopy classes produces function. These three levels are not separate phenomena but successive expressions of the same underlying process: the structured collapse of possibility space.

16. Sheaf-Theoretic Emergence of Bundle Geometry

The trajectory-aware representation introduced in earlier sections admits a natural reformulation in the language of sheaf theory. This provides a precise mathematical framework for describing the passage from local constrained dynamics to global geometric structure.

16.1. The Configuration Sheaf

Let $\Omega \times [0, T]$ denote spacetime, equipped with an open cover $\{U_i\}_{i \in I}$. To each open set $U \subset \Omega \times [0, T]$, we associate the set

$$\mathcal{F}(U) := \{(\Phi, \mathbf{v}, \mathcal{S}) \text{ on } U \mid \text{admissible}\}.$$

This defines a presheaf $\mathcal{F} : \mathbf{Open}(\Omega \times [0, T])^{\mathrm{op}} \to \mathbf{Set}$, with restriction maps given by field restriction.

Proposition 16.1. *$\mathcal{F}$ is a sheaf of admissible configurations.*

Sketch. Locality holds by construction. For gluing, if a family $\{\mathcal{X}_i \in \mathcal{F}(U_i)\}$ agrees on overlaps $U_i \cap U_j$, then there exists a unique global field $\mathcal{X} \in \mathcal{F}(\bigcup_i U_i)$ obtained by patching. □

In practice, admissibility is only approximate, and gluing may fail. This failure is captured by cohomological obstruction classes.

16.2. Cohomological Obstructions

Given a cover $\{U_i\}$ and local sections $\mathcal{X}_i \in \mathcal{F}(U_i)$, define the mismatch on overlaps:

$$\delta_{ij} = \mathcal{X}_i|_{U_i \cap U_j} - \mathcal{X}_j|_{U_i \cap U_j}.$$

The collection $\{\delta_{ij}\}$ defines a Čech 1-cochain with values in the sheaf of differences. Consistency requires that this cochain be a cocycle, and triviality of its cohomology class ensures the existence of a global section.

Proposition 16.2. *The obstruction to global reconstruction of $\mathcal{X}$ is measured by the cohomology class $[\delta] \in \check{H}^1(\{U_i\}, \mathcal{F})$.*

Thus, global structure is not assumed, but arises when cohomological obstructions vanish or become negligible under coarse-graining.

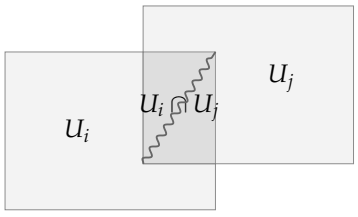

Figure 5: A nonzero overlap mismatch δ_{ij} defines a Čech 1-cochain; its cohomology class measures the obstruction to assembling local sections into a global field.

16.3. Coarse-Graining as a Contravariant Functor

Let $\mathcal{U}$ denote a fine cover and $\mathcal{V}$ a coarser cover of spacetime. Coarse-graining induces a map π :

$\mathcal{U} \to \mathcal{V}$ and therefore a morphism of sites. This defines a contravariant functor on sheaves

$$\pi^* : \mathrm{Sh}(\mathcal{V}) \longrightarrow \mathrm{Sh}(\mathcal{U}),$$

together with a pushforward

$$\pi_* : \mathrm{Sh}(\mathcal{U}) \longrightarrow \mathrm{Sh}(\mathcal{V}).$$

The effective coarse-grained configuration is given by $\overline{\mathcal{F}} := \pi_* \mathcal{F}$.

Remark 16.3. *The functor π_* integrates out fine-scale variability while preserving global consistency data encoded in cohomology.*

16.4. Derived Structure and Accessibility Collapse

The configurational accessibility field $\mathcal{S}$ governs the complexity of the sheaf $\mathcal{F}$. In regimes of high $\mathcal{S}$, the sheaf admits many distinct local sections and nontrivial cohomology. As $\mathcal{S}$ decreases, admissible configurations are restricted and the sheaf simplifies: higher cohomology groups become trivial, and the sheaf approaches one with fewer generators and simpler gluing data.

Proposition 16.4. *In the low-accessibility regime, higher cohomology groups of $\mathcal{F}$ collapse, and the sheaf becomes effectively locally constant with respect to the coarse cover.*

16.5. Emergence of Bundle Geometry

When cohomological obstructions are suppressed and the sheaf simplifies, the remaining structure can be described by a fiber bundle. The sheaf $\overline{\mathcal{F}}$ determines a base space given by spacetime, fibers given by residual admissible configurations, and transition functions derived from overlap data. The transport field $\mathbf{v}$ induces a connection on this bundle, while variations in Φ generate curvature.

Proposition 16.5 (Emergent Bundle Structure)**.** *In the limit of strong accessibility collapse, the coarse-grained sheaf $\overline{\mathcal{F}}$ determines a fiber bundle with connection, whose curvature encodes the residual constraint structure of the system.*

More precisely: in the limit $\mathcal{S} \to 0$, the configuration sheaf admits a unique global section, up to isomorphism, compatible with all overlaps, and its residual symmetry reduces to a structure group acting on fibers. Bundle geometry is therefore not assumed but is the terminal object of accessibility collapse: the unique structure that remains when all admissible alternatives have been foreclosed.

This construction provides a precise sense in which geometric unity emerges from constrained dynamics. The bundle structure is not fundamental but arises as the global organization of a sheaf of local configurations under coarse-graining and accessibility collapse. Geometric unity corresponds to the regime in which the configuration sheaf reduces to a bundle with connection, and dynamics are governed by its associated curvature.

16.6. Higher Sheaf Structure and Trajectory Memory

In regimes of high configurational accessibility, the configuration sheaf $\mathcal{F}$ should properly be regarded as a higher sheaf, or derived stack, with nontrivial higher gluing data encoding trajectory memory. The non-Markovian memory kernels $\mathcal{M}_i$ introduced in Section 8 represent precisely this higher data: they encode how local trajectory fragments must be consistently assembled across overlaps in a way that a 1-sheaf, which tracks only field values and their immediate compatibility, cannot capture. Accessibility collapse corresponds to truncation of this higher sheaf to a 1-sheaf, as the system loses the topological diversity that made higher gluing data necessary. The derived-to-classical transition is therefore not merely a computational simplification but a structural consequence of $\mathcal{S} \to 0$: when few futures remain, the memory of alternative pasts becomes irrelevant to global coherence.

Proposition 16.6 (Bundle Emergence as Terminal Descent Object)**.** *Let $\mathcal{F}$ be the configuration sheaf and suppose that for a coarse cover $\mathcal{V}$, $\check{H}^k(\mathcal{V}, \mathcal{F}) = 0$ for all $k \geq 1$. Then $\mathcal{F}$ is equivalent to the sheaf of sections of a fiber bundle with structure group G acting on the residual admissible fiber.*

This replaces the earlier philosophical statement with a standard descent condition: bundle geometry is not assumed but is the unique structure that remains once all higher cohomological obstructions have vanished.

Remark 16.7 (Equivalence of Functional Regimes)**.** *Up to coarse-graining, the following conditions are equivalent signatures of functional lock-in: persistent low configurational accessibility $\mathcal{S}$; reduction in admissible homotopy classes; vanishing higher sheaf cohomology $\check{H}^k = 0$ for $k \geq 1$; and emergence of a bundle description with structure group G. This equivalence*

constitutes the unified interpretation of function across all domains treated in the paper.

17. Lorentz Transformations as Sheaf Automorphisms

The projection-based language developed above must remain consistent with relativistic causality. In particular, it must not imply faster-than-light propagation. This is ensured by the fact that Lorentz transformations act as automorphisms of the projection functor from the configuration sheaf to observer coordinate spaces, not on the underlying events or trajectories themselves.

17.1. Invariant Structure

In special relativity, the invariant object is the spacetime interval $s^2 = c^2t^2 - \|x\|^2$. Observers may disagree about temporal and spatial coordinates, but they agree on the interval. Within the present framework, this corresponds to an invariant admissibility condition on trajectories. A trajectory γ is not defined by a single observer's projection, but by the equivalence class of all projections that preserve its invariant structure.

17.2. Observers as Local Sections

An observer corresponds to a local section of the configuration sheaf. Given a trajectory γ, observer α assigns a projected representation $\Pi_\alpha(\gamma) = (t_\alpha, x_\alpha)$, while observer β assigns $\Pi_\beta(\gamma) = (t_\beta, x_\beta)$. Both are representations of the same underlying trajectory. A Lorentz transformation is therefore a map

$$\Lambda_{\alpha\beta} : \Pi_\alpha(\gamma) \longrightarrow \Pi_\beta(\gamma)$$

that preserves the invariant interval.

17.3. Lorentz Transformations as Automorphisms

In sheaf-theoretic terms, Lorentz transformations act as automorphisms of the sheaf of observer-projections, changing local coordinate descriptions while preserving the global admissibility structure:

$$\Lambda^*_{\alpha\beta}\mathcal{I}[\gamma] = \mathcal{I}[\gamma].$$

Thus Lorentz transformations deform the image of a trajectory under projection, not the trajectory itself.

17.4. Time Dilation as Projection Distortion

For two events occurring at the same spatial location in the comoving frame, the proper time is $\tau = t_0$. An observer who sees the system moving with speed v measures

$$t = \frac{t_0}{\sqrt{1 - v^2/c^2}}.$$

This does not mean that the event itself has changed. Rather, the same invariant trajectory is being represented through a different section of the observer sheaf. The standard light-clock derivation expresses this as $(ct)^2 = (vt)^2 + (ct_0)^2$, so that $t = \gamma(v)t_0$ with $\gamma(v) = (1 - v^2/c^2)^{-1/2}$. The diagonal path is longer in the projected image not because the underlying causal trajectory has become superluminal, but because the observer's slicing has tilted relative to the intrinsic trajectory.

17.5. No Superluminal Consequence

A trajectory is admissible only if it is timelike or null: $c^2t^2 - \|x\|^2 \geq 0$. Because Lorentz transformations preserve this quantity, they preserve causal type.

Proposition 17.1 (No Superluminal Propagation)**.** *If a trajectory is timelike or null in one frame, then it remains timelike or null in every Lorentz-related frame. Therefore no Lorentz transformation can convert a subluminal trajectory into a superluminal one.*

Proof. Lorentz transformations preserve the spacetime interval. Since the sign of the interval determines whether a trajectory is timelike, null, or spacelike, causal classification is invariant under the transformation. □

Faster-than-light travel would require changing the invariant causal structure, not merely changing the projection. Such a change is excluded by the framework. Lorentz transformations deform the representation of a trajectory, not the event or trajectory itself.

18. Lorentz Invariance from an RSVP-Style Trajectory Functional

We now show how the relativistic invariant can be expressed within the constraint–transport–accessibility language of the present framework. The goal is not to replace special relativity but to show that Lorentz invariance appears as a symmetry of admissible trajectories.

18.1. Trajectory Functional

Let a trajectory through spacetime and configuration space be written as

$$\gamma : \tau \mapsto (x^\mu(\tau), \Phi(\tau), \mathbf{v}(\tau), \mathcal{S}(\tau)),$$

where τ denotes intrinsic progression along the trajectory. We define an effective trajectory action coupling proper-time length to the RSVP fields:

$$\mathcal{A}_{\text{RSVP}}[\gamma] = \int \Big[\sqrt{c^2 \dot{t}^2 - \|\dot{\mathbf{x}}\|^2} + V_\Phi(\Phi) + \tfrac{1}{2}\mu(\Phi)\, g_{\mu\nu} v^\mu v^\nu - \lambda \mathcal{S} \Big] d\tau, \quad (8)$$

where $V_\Phi(\Phi)$ encodes structural constraint, $\mu(\Phi) g_{\mu\nu} v^\mu v^\nu$ encodes transport cost, and $-\lambda\mathcal{S}$ encodes configurational accessibility.

18.2. Admissibility Constraint

Relativistic causality imposes $c^2\dot{t}^2 - \|\dot{\mathbf{x}}\|^2 \geq 0$, equivalently $\|\dot{\mathbf{x}}\| \leq c\dot{t}$. Thus admissible trajectories are those whose spacetime projection is timelike or null. In RSVP language, the physical transport component satisfies $\|\mathbf{v}_{\text{phys}}\| \leq c$.

18.3. Lorentz Symmetry of the Action

Let Λ be a Lorentz transformation. Then $c^2 dt^2 - d\mathbf{x}^2 = c^2 dt'^2 - d\mathbf{x}'^2$, so the square root term in equation (8) is invariant. If Φ and $\mathcal{S}$ are treated as Lorentz scalars and v^μ as a four-vector, the full action is invariant under Λ, giving the Lorentz-covariant form

$$\mathcal{A}_{\text{RSVP}}[\gamma] = \int \big[ds + V_\Phi(\Phi)\, d\tau + \tfrac{1}{2}\mu(\Phi)\, g_{\mu\nu} v^\mu v^\nu\, d\tau - \lambda \mathcal{S}\, d\tau \big],$$

where $ds^2 = g_{\mu\nu} dx^\mu dx^\nu$.

Proposition 18.1 (Lorentz Invariance of Admissible Trajectories)**.** *The set of admissible RSVP trajectories is invariant under Lorentz transformations whenever the RSVP action is constructed from Lorentz-scalar field combinations.*

Proof. Lorentz transformations preserve the Minkowski metric: $\Lambda^\top g \Lambda = g$. Therefore $g_{\mu\nu}\dot{x}^\mu \dot{x}^\nu$ is invariant. Since admissibility is defined by the sign of this quantity, the admissible set is preserved. If the field couplings are Lorentz scalars, the action is also invariant. □

18.4. Time Dilation Recovered

For a trajectory with spatial velocity v, the invariant interval gives $d\tau^2 = dt^2(1 - v^2/c^2)$, so $dt = d\tau(1 - v^2/c^2)^{-1/2}$. The usual Lorentz factor $\gamma(v) = (1 - v^2/c^2)^{-1/2}$ is recovered. In the present interpretation, $\gamma(v)$ measures projection distortion: the factor by which an observer-section elongates the image of an invariant trajectory when that trajectory has transverse transport relative to the frame.

19. Causality as a Sheaf-Theoretic Admissibility Constraint

The previous section established that Lorentz invariance arises as a symmetry of admissible trajectories. We now refine this result by showing that causality itself can be interpreted as a sheaf-theoretic constraint on the existence of global sections.

19.1. The Admissible Subsheaf

For each open set $U \subset \Omega \times [0, T]$, define

$$\mathcal{F}_{\text{adm}}(U) := \{ \mathcal{X} \in \mathcal{F}(U) \mid g_{\mu\nu}\dot{x}^\mu \dot{x}^\nu \geq 0 \}.$$

This defines a subsheaf $\mathcal{F}_{\text{adm}} \subset \mathcal{F}$ consisting of locally admissible configurations. Stability under restriction follows immediately: if $\mathcal{X}$ satisfies the causality constraint on U, its restriction to any $V \subset U$ does also.

19.2. Global Admissibility and Gluing

A global trajectory exists if and only if a compatible family of local sections $\{\mathcal{X}_i \in \mathcal{F}_{\text{adm}}(U_i)\}$ can be glued into a single section over $\bigcup_i U_i$. Gluing is obstructed if the local data implies inconsistent causal structure across overlaps.

Definition 19.1 (Causal Compatibility)**.** *A family $\{\mathcal{X}_i\}$ is causally compatible if on each overlap $U_i \cap U_j$, the induced trajectories agree both as fields and as elements of $\mathcal{F}_{\text{adm}}$.*

Proposition 19.2. *A global admissible trajectory exists if and only if the associated Čech 1-cocycle of mismatches vanishes in $\check{H}^1(\{U_i\}, \mathcal{F}_{\text{adm}})$.*

19.3. Exclusion of Superluminal Patching

Suppose one attempts to construct a trajectory that is locally admissible in each patch but globally superluminal. This would require that on

overlaps $U_i \cap U_j$, the local sections agree as fields but disagree in causal classification. Such a mismatch would produce a nontrivial cohomology class $[\delta] \neq 0$, preventing the existence of a global section.

Proposition 19.3 (No Superluminal Gluing)**.** *There exists no global section of $\mathcal{F}$ whose local restrictions are timelike in each patch but collectively define a spacelike trajectory.*

Sketch. If such a section existed, it would define a global trajectory violating $g_{\mu\nu}\dot{x}^\mu\dot{x}^\nu \geq 0$. However, local admissibility enforces this inequality in each patch. Violation at the global level would require inconsistent gluing, which is obstructed by the sheaf condition. Therefore no such global section exists. □

Causality is therefore not merely a local inequality but a global consistency condition on the sheaf of configurations. Superluminal motion would correspond not to a different projection but to attempting to extend a locally admissible section beyond the domain where the sheaf condition holds; the obstruction is not energetic but categorical — the extension fails to exist. The speed of light is not a dynamical limit imposed on trajectories, but a structural boundary enforced by the existence of global sections.

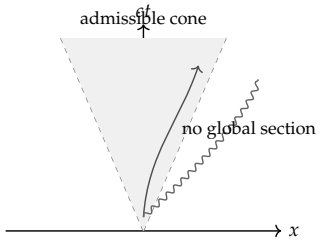

Figure 6: Superluminal patching fails because spacelike extension lies outside the admissible subsheaf. The causal boundary is a structural property of gluing, not a dynamical speed limit.

20. Projection Geometry and the Interpretation of Time Dilation

We now return to the interpretation of time dilation in light of the preceding formalism.

20.1. Trajectory Versus Representation

Let γ be a fixed admissible trajectory. Observers α and β assign projections $\Pi_\alpha(\gamma) = (t_\alpha, x_\alpha)$ and $\Pi_\beta(\gamma) = (t_\beta, x_\beta)$. These are not different trajectories but different coordinate representations of the same object.

20.2. Geometric Origin of Time Dilation

The light-clock construction yields $(ct)^2 = (vt)^2 + (ct_0)^2$, which implies $t = \gamma(v)t_0$. This relation is geometric: it arises from the metric structure of spacetime. In the present framework, it reflects the fact that projection operator Π_α slices the trajectory at an angle relative to Π_β. Let intrinsic progression along γ be parameterized by τ, so $d\tau^2 = dt^2 - dx^2/c^2$. Transport through the vector field $\mathbf{v}$ introduces transverse components in the projected representation, increasing the apparent length of the trajectory. Observed time is the length of a projected trajectory; proper time is the intrinsic length of the trajectory itself.

20.3. No Physical Slowing of Time

This resolves the common misconception that time slows down for moving objects. The trajectory γ does not change, the invariant length τ does not change, and only the projection changes. Time dilation is not a change in physical evolution but a change in how that evolution is represented.

The projection-based interpretation is therefore conservative with respect to relativity. The same admissible trajectory is seen differently by different observers, but its causal and geometric structure remains unchanged. This aligns naturally with the broader framework: projection operators Π_k correspond to observers, sheaf structure encodes consistency across projections, and trajectory invariants define admissibility.

21. Metric Curvature from Spatial Variation of Constraint

The preceding sections treated Lorentz invariance in the flat-spacetime limit, where admissible trajectories are governed by a fixed Minkowski metric. We now indicate how the same framework extends toward curved spacetime by allowing the constraint field Φ to modify the effective metric experienced by trajectories.

21.1. From Fixed Metric to Effective Metric

In special relativity, admissibility is defined by $\eta_{\mu\nu}\dot{x}^\mu\dot{x}^\nu \geq 0$, where $\eta_{\mu\nu}$ is the Minkowski metric. In a constrained-field setting, the scalar field

$\Phi(x)$ may alter the local geometry of admissibility. We therefore introduce an effective metric

$$g^{\text{eff}}_{\mu\nu}(x) = g_{\mu\nu}\big(\Phi(x), \nabla\Phi(x), \mathcal{S}(x)\big),$$

so that causal admissibility becomes $g^{\text{eff}}_{\mu\nu}(x)\dot{x}^\mu\dot{x}^\nu \geq 0$. The effective metric is not identified with the constraint field itself but arises as the unique, up to equivalence, local bilinear form compatible with admissibility under the constraint–transport–accessibility coupling. Curvature arises from spatial variation in the constraint structure rather than being imposed externally. In the flat limit $\Phi = \text{const}$, $g^{\text{eff}}_{\mu\nu} \to \eta_{\mu\nu}$, recovering special relativity.

21.2. Constraint Gradients as Curvature Sources

If Φ varies slowly, write the effective metric as a perturbation of the flat metric: $g^{\text{eff}}_{\mu\nu} = \eta_{\mu\nu} + h_{\mu\nu}[\Phi]$, where to lowest order

$$h_{\mu\nu}[\Phi] = a\,\Phi\,\eta_{\mu\nu} + b\,\partial_\mu\Phi\,\partial_\nu\Phi + c\,\nabla_\mu\nabla_\nu\Phi,$$

for phenomenological coefficients a, b, c. The first term rescales local interval structure, the second introduces directional anisotropy from gradients of constraint, and the third encodes curvature-like response to second-order spatial variation.

21.3. Geodesics as Constraint-Compatible Trajectories

Given the effective metric, admissible free trajectories extremize the proper-time functional $\tau[\gamma] = \int_\gamma \sqrt{g^{\text{eff}}_{\mu\nu}dx^\mu dx^\nu}$. The resulting equations are the geodesic equations

$$\frac{d^2x^\mu}{d\tau^2} + \Gamma^\mu_{\alpha\beta}\frac{dx^\alpha}{d\tau}\frac{dx^\beta}{d\tau} = 0,$$

where $\Gamma^\mu_{\alpha\beta}$ are the Christoffel symbols of $g^{\text{eff}}_{\mu\nu}$. In the constrained-field interpretation, these are trajectories of least distortion through the admissibility geometry determined by Φ. Gravitational curvature corresponds to spatial variation in the geometry of admissibility.

21.4. Relation to the Einstein Field Equations

A complete recovery of general relativity would require specifying the dynamical relation between Φ and the effective metric. Formally, one may introduce an action

$$\mathcal{A} = \int \left[\frac{1}{16\pi G}R(g^{\text{eff}}) + \mathcal{L}_{\Phi,\mathbf{v},\mathcal{S}} + \mathcal{L}_{\text{matter}}\right]\sqrt{-g^{\text{eff}}}\,d^4x,$$

where $R(g^{\text{eff}})$ is the scalar curvature. Variation with respect to $g^{\text{eff}}_{\mu\nu}$ gives equations of the form

$$G_{\mu\nu}(g^{\text{eff}}) = 8\pi G\left(T^{\text{matter}}_{\mu\nu} + T^{\Phi,\mathbf{v},\mathcal{S}}_{\mu\nu}\right),$$

where $T^{\Phi,\mathbf{v},\mathcal{S}}_{\mu\nu}$ represents the contribution of constraint, transport, and accessibility fields to the effective geometry.

21.5. Weak-Field Limit

In the weak-field, slow-motion limit, $g^{\text{eff}}_{00} \approx 1 + 2\varphi/c^2$, where φ is the Newtonian gravitational potential. In the constrained-field interpretation, φ may be modeled as a coarse-grained projection of Φ: $\varphi = \mathcal{P}[\Phi]$ for some projection or averaging operator $\mathcal{P}$. The geodesic equation then reduces to $d^2\mathbf{x}/dt^2 = -\nabla\varphi$, so gravitational acceleration appears as motion along gradients of the projected constraint field.

21.6. No Violation of Relativistic Causality

Because admissibility is still defined by $g^{\text{eff}}_{\mu\nu}\dot{x}^\mu\dot{x}^\nu \geq 0$, curvature does not permit superluminal propagation. It changes the structure of admissible trajectories but does not remove the causal boundary.

Proposition 21.1 (Curved Causal Admissibility)**.** *If the effective metric $g^{\text{eff}}_{\mu\nu}$ is Lorentzian, then causal classification remains well-defined locally, and admissible trajectories remain timelike or null with respect to g^{eff}.*

Proof. A Lorentzian metric defines a local light cone at each point. Curvature changes the orientation and structure of cones across spacetime, but not the local distinction between causal and noncausal directions. □

The passage from special to general relativity is therefore interpreted as the transition from a fixed admissibility geometry to a spatially varying one: $\eta_{\mu\nu} \longrightarrow g^{\text{eff}}_{\mu\nu}(\Phi, \nabla\Phi, \mathcal{S})$. Special relativity corresponds to the case where Φ is uniform and the admissibility geometry is flat; general relativity corresponds to the case where the geometry of admissibility varies across spacetime. Curvature is the deformation of the admissibility geometry induced by nonuniform constraint.

22. A Causal Example: Collagen Peptide Gelation

Consider a collagen peptide network undergoing gelation in aqueous solution. The experimental ob-

jective is to determine whether an imposed preparation variable—ionic strength—causally changes the final mechanical stiffness of the network, and whether this effect is mediated by mesoscale changes in aggregation, fiber bundling, and transport accessibility.

Let the treatment variable be $A \in \{a_0, a_1\}$, where a_0 denotes a low-ionic-strength condition and a_1 denotes a high-ionic-strength condition. Let the observed outcome be the storage modulus $Y = G'$ measured after gelation by oscillatory rheology. The causal estimand is the average treatment effect

$$\tau = \mathbb{E}[Y(a_1) - Y(a_0)],$$

where $Y(a)$ denotes the stiffness that would be observed if the system were prepared under condition a.

Within the constrained-field framework, the treatment does not act directly on Y. Instead, it perturbs the field evolution, writing $\mathcal{X}(x,t;A) = \big(\Phi(x,t;A), \mathbf{v}(x,t;A), \mathcal{S}(x,t;A)\big)$. Here Φ represents collagen peptide aggregation and local fiber density, $\mathbf{v}$ represents transport and alignment during gelation, and $\mathcal{S}$ represents configurational accessibility. Ionic strength modifies the local interaction term $f_{\mathrm{loc}}(\Phi; A)$ in the free-energy functional, altering which aggregates nucleate, how rapidly fibers bundle, how transport pathways close, and when the system loses configurational accessibility. The treatment therefore acts upstream of structure. The final modulus is the mechanical expression of a completed trajectory, specifically one that has entered a low-$\mathcal{S}$ regime in which configurational accessibility has collapsed and network rearrangement is no longer dynamically available:

$$G' = \mathcal{R}\left[\{\Phi(t), \mathbf{v}(t), \mathcal{S}(t)\}_{t=0}^{T}\right].$$

22.1. Trajectory Dependence and TARTAN

Collagen peptide networks are path-dependent. Two samples may have similar final density but different assembly histories, leading to different network topology and stiffness. Instead of summarizing the system only by $\Phi(\cdot, T)$, we cover the gelation trajectory by overlapping temporal patches $U_i = [t_i, t_{i+1}]$, assign to each patch a local field history $\mathcal{X}_i$, and enforce overlap consistency. This prevents the model from treating gelation as a Markovian sequence of unrelated snapshots. Early nucleation, intermediate bundling, and late network locking are represented as overlapping trajectory fragments with a history-consistency score

$$H_k = \sum_i \|\mathcal{X}_{i,k} - \widehat{\mathcal{X}}_{i,k}\|^2 + \sum_{i,j} \|\rho_{ij}(\mathcal{X}_{i,k}) - \rho_{ji}(\mathcal{X}_{j,k})\|^2.$$

22.2. Statistical Model

A practical regression model is

$$G'_k = \beta_0 + \beta_A A_k + \int_0^T \beta_M(t)\, M_k(t)\, dt + \beta_H H_k + \epsilon_k,$$

where k indexes samples, $M_k(t) = (\xi(t), r_f(t), \alpha(t), c(t))$ contains measured structural summaries (correlation length, fiber radius, anisotropy index, connectivity), and H_k is the history-consistency score. A significant β_A after adjustment for $M(t)$ and H indicates a direct effect of ionic strength not explained by observed structure. A significant β_H indicates that assembly history contributes to stiffness beyond static morphology—precisely the regime where trajectory-aware representation is indispensable.

22.3. Testing for Accessibility Collapse

The constraint-induced collapse mechanism in equation (7) predicts that ionic strength changes the rate at which the system enters a low-$\mathcal{S}$ regime. This can be tested by designing two preparation protocols that produce similar final scattering profiles but different assembly paths—for example, one condition rapidly screening electrostatic repulsion early in gelation, another gradually increasing ionic strength. If the final $\Phi(\cdot, T)$ appears similar but the measured moduli differ, the network carries non-Markovian memory and the assembly path has causal relevance. The corresponding statistical test adds $\beta_H H_k$ to a baseline model containing only final-structure summaries; significance of β_H after this adjustment would confirm that $\mathcal{S}$ history, not just Φ geometry, determines function.

23. Implications for Experiment and Design

The unified framework has direct consequences for how mesoscale systems are studied and engineered. The emphasis shifts from identifying stable structures and correlating them with properties to controlling trajectories in configuration space.

Design as trajectory control. Because function corresponds to stabilized evolution of $\mathcal{X}(x,t)$ within a low-$\mathcal{S}$ basin, design becomes the problem

of steering the system into a desired dynamical regime. Let $\mathcal{U}$ denote a set of admissible controls (temperature, ionic strength, shear, chemical inputs). Then the design problem can be formulated as

$$\min_{u(\cdot)\in\mathcal{U}} \ \mathcal{J}\big[\mathcal{X}(\cdot;u)\big],$$

where $\mathcal{J}$ is an objective functional encoding desired outcomes such as mechanical strength, conductivity, or permeability. Unlike classical optimization over static configurations, this formulation optimizes over trajectories in configuration space.

From this perspective, the design of functional materials can be interpreted as the controlled reduction of configurational accessibility along specific trajectories. Processes such as cross-linking, crystallization, alignment, and templating may be viewed as mechanisms for inducing accessibility collapse in targeted regions of configuration space. Biological systems achieve similar effects through sequence-encoded folding pathways and cooperative assembly. While this interpretation is not exhaustive, it provides a unifying lens through which diverse fabrication and selection processes can be understood.

Experimental strategy. Experiments should be structured to probe sensitivity to trajectory rather than only final state. Key strategies include time-resolved measurements such as SAXS, SANS, and microscopy [29, 21]; controlled perturbations during evolution; comparison of protocols yielding similar final structure but different histories; and reconstruction of trajectory patches from partial observations. These approaches align naturally with the projection framework described in Section 9 and the trajectory-aware representation of Section 8.

Cross-domain transfer. Because the governing structure is shared, insights from one domain can be transferred to another. Methods developed to control anisotropy in polymer networks may inform the design of biological scaffolds, while interfacial stabilization strategies in emulsions may inform membrane engineering.

Proposition 23.1 (Transferability)**.** *If two systems are governed by functionals of similar form, then control strategies that modify trajectories in one system can be adapted to the other under appropriate scaling.*

24. Modular Externalization, Residue Reuse, and State-Space Expansion

The constrained-field framework developed for mesoscale physical systems admits a direct extension to socio-technical and computational systems. In these domains, the fields $(\Phi, \mathbf{v}, \mathcal{S})$ do not represent material aggregation and transport alone, but organizational constraint, workflow propagation, and the space of admissible transformations across distributed systems.

24.1. Modularization as Constraint Redistribution

Modern systems—software platforms, economic networks, and institutional structures—are characterized by modular decomposition. A complex process is partitioned into subcomponents, each governed by local rules and interfaces. Within the present framework, this corresponds to a redistribution of the constraint field Φ across system boundaries.

Definition 24.1 (Modular Externalization)**.** *A system externalizes constraint when it partitions a global process into modules $\{U_i\}$ such that each module carries a localized constraint field Φ_i, while inter-module interactions are mediated through reduced interface constraints.*

This operation does not eliminate constraint; it relocates it. The internal complexity of a module may decrease, but the global system inherits new dependencies encoded in the overlap conditions between modules. In sheaf- theoretic terms, modularization replaces a single global section with a collection of local sections whose compatibility must be enforced across interfaces.

24.2. Residue as Latent Admissible Structure

A characteristic feature of modular systems is the production of byproducts: unused computation, data exhaust, waste heat, or partially completed transformations. These residues are often treated as inefficiencies, yet in many systems they become inputs to new processes.

Definition 24.2 (Admissible Residue)**.** *A residue is admissible if it can be reinterpreted as a valid input to a distinct transformation without violating the constraint structure of the receiving module.*

Admissible residues function as latent trajectory fragments. Within the trajectory-aware representa-

tion, they correspond to partial paths in configuration space that were not completed within one module but remain consistent with admissibility conditions elsewhere. Reuse of residue is therefore equivalent to reattaching previously discarded trajectory segments into new admissible paths.

24.3. Orthograde Transformations and Low-Interference Directions

New transformations in modular systems preferentially arise along directions that do not disrupt existing constraint structures.

Definition 24.3 (Orthograde Transformation)**.** *A transformation is orthograde if it extends system functionality along a direction that preserves local admissibility and minimizes interference with existing constraint fields.*

Orthograde transformations correspond to low-coupling directions in the space of admissible fluxes $\mathbf{v}$. They are the directions along which new modules, services, or processes can be added without requiring global reconfiguration. In algebraic terms, they approximate orthogonality with respect to the bilinear form induced by the constraint structure.

24.4. Local Constraint Reduction and Global State Expansion

A central consequence of modular externalization is a divergence between local and global measures of complexity.

Proposition 24.4 (Local Constraint, Global Expansion)**.** *Modular systems reduce local configurational uncertainty while expanding the global space of admissible configurations through recombination of modules and admissible residues.*

Heuristic Argument. Each module imposes constraints that reduce local $\mathcal{S}$. However, the composition of modules introduces combinatorial degrees of freedom: admissible configurations correspond to compatible selections across modules. If residues remain admissible, they introduce additional partial trajectories that can be recombined, increasing the effective global $\mathcal{S}$ even as local values decrease. □

This result does not violate thermodynamic principles. Rather, it reflects a redistribution of accessibility: uncertainty-like measures decrease locally due to constraint, while the number of globally reachable configurations increases through combinatorial composition. Systems compete by minimizing their own constraint cost while increasing the total space of recomposable trajectories they can access or control, which is why platform structures consistently outperform point-solutions: they do not merely optimize a process but own the adjacency structure of possible processes.

24.5. Failure Modes: Non-Admissible Externalization

Not all externalization produces beneficial expansion. If residues cannot be reintegrated because they violate admissibility conditions or require prohibitive reconstruction, then they do not contribute to global state-space growth.

Proposition 24.5 (Dead Residue)**.** *Residues that cannot be embedded into admissible trajectories act as sinks of configurational accessibility and do not contribute to functional expansion.*

Such residues correspond to irrecoverable waste, technical debt, or incompatible interfaces. They increase local disorder without expanding the global space of useful configurations, and therefore degrade system functionality. The distinction between productive and dead externalization is whether the residue remains admissible for recombination—the difference between a data exhaust pipeline and pollution, or between reusable abstractions and technical debt.

25. Recency, Locality, and the Bitter Lesson

The trajectory-aware framework provides a structural account of recency weighting—a ubiquitous heuristic in learning systems, caching architectures, and human cognition—and connects it to the empirical observation that large-scale, compute-driven learning methods systematically outperform methods that rely on hand-crafted structure.

25.1. Recency as Local Admissibility Projection

In the RSVP framework, the admissibility log $\mathcal{L}$ maintains a full record of past events. Full reconstruction from this log is, in general, expensive: it requires evaluating global gluing consistency across the entire history. Recency weighting provides a low-cost approximation by assigning

$$\text{weight}(e_k) \propto e^{-\lambda(t_n - t_k)},$$

discarding events beyond an effective horizon. This is not merely a heuristic. More recent events sit inside the current admissible basin, have not yet been invalidated by constraint evolution, and are more likely to glue consistently with the current local section of the configuration sheaf. Recency weighting therefore approximates the projection of the full admissibility log onto the current local tangent space of valid trajectories.

Proposition 25.1 (Recency as Local Admissibility Projection)**.** *Time-weighted recency bias approximates the projection of the admissibility log onto the locally coherent trajectory subspace, minimizing gluing obstructions and enabling stable real-time inference.*

Older events are more likely to lie in different homotopy classes from the current trajectory; newer events are more likely to be locally compatible. Recency therefore minimizes expected gluing failure by discarding high-cost, low-relevance historical branches. Responsiveness—the property of a system that updates reliably under new information—is in this sense inversely proportional to expected gluing failure.

Proposition 25.2 (Recency as Minimal Obstruction Estimator)**.** *Let $\mathcal{L}$ be an admissibility log and let $\widehat{\mathcal{L}}_\tau$ be its truncation to the interval $[t-\tau, t]$. Under a decay condition on constraint evolution—specifically, that older events are exponentially less likely to remain in the current admissible basin—the truncated log $\widehat{\mathcal{L}}_\tau$ minimizes expected gluing obstruction among all fixed-length summaries of $\mathcal{L}$.*

This ties the recency heuristic directly to gluing optimality: exponential weighting is not arbitrary but is the natural choice when constraint fields evolve with bounded relaxation rate.

25.2. Locality Constraints and Scaling Behavior

Sutton's Bitter Lesson establishes that methods which scale with compute and data consistently outperform methods that rely on handcrafted structure. The RSVP interpretation of this result is as follows. Hand-crafted structure corresponds to hard-coded constraints on admissible trajectories: the system's configuration space is pre-restricted by design. Scalable methods instead explore a broad trajectory space with weak priors, allowing structure to emerge from data.

The difficulty is that broad exploration drives $\mathcal{S}$ toward high values: many trajectories remain admissible, optimization becomes unstable, and signal is diluted by combinatorial expansion. Recency weighting resolves this by imposing a locality constraint: the effective trajectory space is truncated to a recent neighborhood, preserving local coherence without reverting to hand-crafted global structure.

Proposition 25.3 (Scaling Compatibility via Locality)**.** *Systems that maintain performance under scale do so by enforcing locality constraints—such as recency weighting—that bound effective configurational accessibility, preserving tractable trajectory coherence as global capacity increases.*

The Bitter Lesson therefore requires two ingredients, not one. Exploration capacity increases $\mathcal{S}$ globally; locality constraints prevent $\mathcal{S}$ from becoming computationally intractable locally. Recency bias is the simplest possible locality operator that respects causal structure. This same pattern appears in transformer attention, which implements soft recency weighting across context; in reinforcement learning replay buffers, which prioritize recent and high-return transitions; and in human working memory, which is capacity-limited and recency-biased. These are all approximations to the same principle: retain only the portion of the trajectory that still lies within the current admissible basin.

26. A Minimal Synchronization Model of Cosmological Structure

Before developing the full five-dimensional model, we state a minimal, parameter-free version that makes falsifiable predictions without free functions. This version is the benchmark against which the richer model is compared.

26.1. Definition of the Synchronization Field

We define a higher-dimensional binary coherence field

$$\sigma : \mathbb{R}^3 \times \mathbb{R} \times \Xi \to \{-1, +1\},$$

where Ξ is a compact internal dimension indexing coherence modes. The observable scalar constraint field is the normalized projection

$$\Phi(x,t) = \frac{1}{|\Xi|} \int_\Xi \sigma(x,t,\xi)\, d\xi.$$

The vector transport field arises from phase gradients: $\mathbf{v}(x,t) = -\nabla\Phi(x,t)$. Configurational accessibility is defined by local internal disagreement: $\mathcal{S}(x,t) = \log(1 + \mathrm{Var}_\xi[\sigma(x,t,\xi)])$.

26.2. Parameter-Free Evolution Law

The synchronization field evolves by nearest-neighbor alignment in the extended space $\mathbb{R}^3 \times \Xi$:

$$\partial_t \sigma(x,\xi) = \operatorname{sign}\big(\Delta_x \sigma(x,\xi) + \Delta_\xi \sigma(x,\xi)\big).$$

This defines a 5D Ising-type model with no tunable coupling constants beyond lattice scale and time normalization.

26.3. Scale-Free Coherence and Flat Rotation Curves

Define the effective potential $\varphi_{\text{eff}}(r) = \Phi(r)$. For circular motion, $v_{\text{rot}}^2(r) = r|d\Phi/dr|$. The only radial profile with no preferred length scale and nonzero radial flux is logarithmic:

$$\Phi(r) = A\log(r/r_0), \qquad \frac{d\Phi}{dr} = \frac{A}{r}, \qquad v_{\text{rot}}^2 = A.$$

Hence $v_{\text{rot}} = \sqrt{A}$, a constant independent of r.

26.4. Baryonic Tully–Fisher Scaling

Define the total baryonic source strength $M_b = \int \rho_b \, d^3x$. Under the minimal assumption that coherence charge $Q_\Phi \propto M_b$, and that the radial coherence amplitude satisfies $A \sim Q_\Phi^{1/2}$, we obtain $v_{\text{rot}}^2 \propto M_b^{1/2}$, hence

$$v_{\text{rot}}^4 \propto M_b.$$

This recovers the baryonic Tully–Fisher relation without inserting a dark matter halo profile or empirical interpolation function. The flatness of rotation curves and the baryonic scaling both arise from scale-free coherence geometry.

26.5. Lensing Prediction

Define the effective metric perturbation $g_{00} = -(1+2\Phi)$, $g_{ij} = (1-2\Phi)\delta_{ij}$. The lensing potential is then directly Φ, and lensing maps correlate with coherence structure rather than strictly with baryonic mass.

26.6. Falsification Criteria

The minimal model makes three parameter-free predictions. First, asymptotically flat rotation curves arise without halo profile tuning; deviations in galaxies with confirmed scale-free coherence environments falsify the model. Second, the non-Markovian gravitational response satisfies $\partial_t \Phi \neq 0$ after a perturbation to ρ_b, with a finite coherence relaxation time. Third, lensing correlates with coherence domains rather than strictly baryonic density, producing measurable deviations from ΛCDM in offset systems. Failure of any condition falsifies the synchronization model as stated.

27. A Synchronization-Based Cosmological Extension

The constrained-field framework developed thus far admits a natural extension to cosmological structure formation by interpreting the scalar constraint field Φ as the coarse-grained projection of a higher-dimensional synchronization process. In this section, we formalize this extension as a five-dimensional Ising-like system whose coarse-grained dynamics reproduce the mesoscale field equations introduced earlier.

27.1. Underlying Synchronization Field

Let spacetime be augmented by an additional internal coordinate ξ, representing a coherence or synchronization dimension. The fundamental degrees of freedom are binary variables $\sigma(x,t,\xi) \in \{-1,+1\}$. We define a Hamiltonian

$$\begin{aligned} H[\sigma] = &-J \sum_{\langle x,x'\rangle,\xi} \sigma(x,\xi)\sigma(x',\xi) \\ &- K \sum_{x,\langle \xi,\xi'\rangle} \sigma(x,\xi)\sigma(x,\xi') \\ &- \lambda \sum_{x,\xi} \sigma(x,\xi)\, \mathcal{E}(x), \end{aligned}$$

where J is the spatial coupling governing structure formation, K is the coherence coupling governing synchronization strength, and $\mathcal{E}(x)$ is an external bias encoding baryonic matter and radiation. The dynamics follow a stochastic relaxation process consistent with detailed balance.

27.2. Projection to Mesoscale Fields

The observable fields $(\Phi, \mathbf{v}, \mathcal{S})$ arise as coarse-grained projections of σ. The structural field is defined as the coherence average $\Phi(x,t) = \langle \sigma(x,t,\xi)\rangle_\xi$. The transport field emerges from spatial gradients of coherence: $\mathbf{v}(x,t) = -\mu(\Phi)\,\nabla\Phi(x,t)$. The configurational accessibility field is defined by the logarithmic density of admissible microstates: $\mathcal{S}(x,t) = \log \Omega(x,t)$, where Ω counts spin configurations consistent with local constraints.

27.3. Continuum Limit and Effective Field Theory

Under coarse-graining, the spin system admits a continuum description in terms of a free-energy functional

$$\mathcal{F}[\Phi] = \int_\Omega \left[-\frac{a}{2}\Phi^2 + \frac{b}{4}\Phi^4 + \frac{\kappa}{2}|\nabla\Phi|^2 \right] dx,$$

recovering the Landau–Ginzburg structure of the mesoscale framework. The resulting evolution equation

$$\partial_t \Phi = D\Delta\Phi - a\Phi - b\Phi^3 + \gamma|\nabla\Phi|^2 + \eta$$

defines the effective large-scale dynamics and provides the bridge between discrete coherence states and continuous mesoscale behavior. Regions of high $|\Phi|$ correspond to synchronized domains, projecting into observable spacetime as galaxies and clusters. Interfaces between domains appear as filaments and void boundaries.

28. Cosmological Predictions from Synchronization Dynamics

The synchronization-based extension yields physical predictions that differ qualitatively from those of ΛCDM and from modified-gravity approaches such as MOND.

28.1. Galaxy Formation as Domain Coarsening

In the absence of strong external bias, the synchronization field undergoes spontaneous symmetry breaking followed by domain coarsening. The characteristic domain size grows as $L(t) \sim t^{1/2}$, consistent with the Allen–Cahn universality class.

Proposition 28.1 (Galaxies as Coherence Domains)**.** *Galaxies correspond to spatial regions in which the synchronization field Φ has converged to a locally stable phase, forming a coherent domain of low configurational accessibility.*

The characteristic size of a galaxy is therefore determined by the correlation length of the synchronization field rather than by virial mass alone.

28.2. Filamentary Structure as Domain Boundaries

Proposition 28.2 (Filaments as Phase Boundaries)**.** *Cosmic filaments arise as domain walls of the synchronization field, representing boundaries between regions of distinct phase alignment.*

Unlike in ΛCDM, where filaments are conduits of matter flow into halos, here they are topological features of the coherence field itself. Matter distribution follows these structures but does not generate them.

28.3. Rotation Curves from Coherence Coupling

Define the spatial correlation function $C(r) = \langle\sigma(0)\sigma(r)\rangle$. The effective rotational velocity is proportional to $v(r) \propto v_0\, C(r)$. If coherence decays slowly, $C(r) \sim r^{-\epsilon}$, then $v(r) \approx$ const.

Proposition 28.3 (Flat Rotation from Long-Range Coherence)**.** *Slow decay of synchronization correlations produces asymptotically flat rotation curves independent of baryonic mass distribution.*

28.4. Environmental Dependence

Proposition 28.4 (Environmental Coherence Effect)**.** *Galaxies embedded in regions of higher large-scale synchronization exhibit enhanced rotational support relative to isolated galaxies of similar baryonic mass.*

This predicts correlations between rotation curve shape and position within the cosmic web, providing a direct observational test not available in MOND.

28.5. Memory Effects and Dwarf Galaxy Variability

Because the synchronization field evolves through domain coarsening with residual metastability, it retains memory of formation history. Post-merger systems may exhibit long-lived deviations from equilibrium predictions. Small systems are more sensitive to fluctuations in Φ, predicting increased scatter in velocity dispersion for dwarf galaxies without requiring additional dark matter components.

29. Gravitational Lensing from Synchronization-Induced Effective Geometry

The synchronization-based extension must reproduce not only galaxy rotation curves but also gravitational lensing. In the present framework, curvature is not fundamental but emerges from spatial variation in Φ.

29.1. Effective Metric from Coherence Fields

We postulate that the observable spacetime metric arises as a functional of the synchronization field and its derivatives:

$$g^{\text{eff}}_{\mu\nu}(x) = \eta_{\mu\nu} + h_{\mu\nu}[\Phi(x), \nabla\Phi(x), \mathcal{S}(x)],$$

where to lowest nontrivial order $h_{\mu\nu} = a\,\Phi\,\eta_{\mu\nu} + b\,\partial_\mu\Phi\,\partial_\nu\Phi + c\,\nabla_\mu\nabla_\nu\Phi$. The effective metric is not identified with the constraint field itself but arises as the unique, up to equivalence, local bilinear form compatible with admissibility under the coupling. In the flat limit $\Phi = \text{const}$, $g^{\text{eff}}_{\mu\nu} \to \eta_{\mu\nu}$.

29.2. Null Geodesics and Light Propagation

Light propagation is determined by null geodesics of $g^{\text{eff}}_{\mu\nu}$. In the weak-field limit, write $g^{\text{eff}}_{00} \approx 1 + 2\varphi/c^2$ and $g^{\text{eff}}_{ij} \approx -(1 - 2\psi/c^2)\delta_{ij}$. The effective potentials are $\varphi \sim \alpha\Phi + \beta|\nabla\Phi|^2$ and $\psi \sim \alpha'\Phi$. The bending angle of light is then

$$\hat{\alpha} = \frac{2}{c^2}\int \nabla_\perp(\varphi + \psi)\,dz,$$

so lensing depends on both the magnitude and spatial variation of Φ, not directly on mass density.

Proposition 29.1 (Lensing from Coherence Gradients)**.** *Gravitational lensing is dominated by spatial gradients of the synchronization field. Galaxy clusters correspond to coherence peaks, filaments to strong gradient regions, and voids to low-coherence regions with weak lensing.*

29.3. Recovery of the Standard Weak Lensing Limit

Assuming baryonic matter induces a bias $\Delta\Phi \sim \rho_{\text{baryon}}$, one recovers $\Delta\varphi \sim \rho_{\text{baryon}}$ to leading order, reproducing Newtonian lensing in the regime where coherence is tightly coupled to matter. Deviations arise when synchronization extends beyond the baryonic distribution, producing apparent lensing not attributable to visible mass.

Relative to ΛCDM, the same observational effect attributed to dark matter halos arises here from extended coherence fields. Relative to MOND, the synchronization framework naturally produces lensing through the same mechanism that generates rotation curves, without requiring a separate relativistic extension.

30. Closure Relation and Forward Observational Model

The central unresolved degree of freedom in the synchronization framework is the mapping between baryonic matter density ρ_b and the coherence field Φ. To recover both dynamical and lensing observables, this mapping must simultaneously reproduce Newtonian gravity in the high-density limit, generate extended coherence beyond baryonic support for dark-like effects, and remain stable under the dissipative dynamics of the RSVP equations.

30.1. Field Equation for Φ

We postulate a nonlinear elliptic equation

$$\Delta\Phi - m^2\Phi + \lambda\Phi^3 = \alpha\rho_b + \gamma|\nabla\Phi|^2, \qquad (9)$$

where m^{-1} sets the coherence decay scale, α controls baryonic sourcing, λ prevents runaway growth, and γ controls self-reinforcement of coherence gradients.

30.2. Effective Gravitational Potential

The observable potential is defined as

$$\varphi_{\text{eff}}(x) = A\Phi(x) + B|\nabla\Phi(x)|^2,$$

where the first term reproduces standard gravity-like behavior and the second generates the extended dark-like contribution. The effective acceleration is $\mathbf{a} = -\nabla\varphi_{\text{eff}} = -A\nabla\Phi - B\nabla(|\nabla\Phi|^2)$.

In the high-density limit, $\Phi \approx (\alpha/m^2)\rho_b$, recovering Newtonian behavior $\mathbf{a} \sim -\nabla\rho_b$. In the low-density outer regions, the gradient term dominates, producing extended acceleration without enclosed mass. If $d\Phi/dr \sim 1/r$, the gradient term contributes a constant to $v^2(r)$, reproducing flat rotation curves without a particle dark matter component. The lensing consistency condition requires $\psi = \varphi$, so the same Φ governs both rotation and lensing with no additional free field.

30.3. Forward Pipeline

The complete observational pipeline maps $\rho_b(x) \to \Phi(x) \to \varphi_{\text{eff}}(x) \to \{v(r), \kappa, \gamma_1, \gamma_2\}$. Given a baryonic density profile (for a disk galaxy, an exponential disk plus optional bulge), one solves equation (9) iteratively until convergence, then computes φ_{eff}, the rotation curve $v^2(R) = R\,\partial\varphi_{\text{eff}}/\partial R$, the lensing

potential $\psi_{\rm lens} = (2/c^2)\int \varphi_{\rm eff}\, dz$, convergence $\kappa = \frac{1}{2}\nabla_\perp^2 \psi_{\rm lens}$, and shear components $\gamma_1 = \frac{1}{2}(\partial_x^2 - \partial_y^2)\psi_{\rm lens}$ and $\gamma_2 = \partial_x \partial_y \psi_{\rm lens}$. The discipline that keeps the model falsifiable is that the same Φ and the same parameters must explain both rotation and lensing simultaneously.

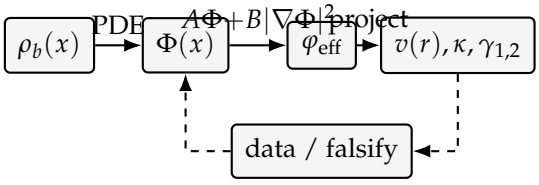

Figure 7: Forward-model pipeline for synchronization cosmology. The same field $\Phi[\rho_b]$ must reproduce both rotation curves and lensing; separate fits would destroy falsifiability.

31. Rotation-Curve Scaling from Scale-Free Synchronization

We derive the asymptotic rotation-curve law implied by the minimal synchronization model and show that it reproduces the baryonic Tully–Fisher relation without free parameters.

31.1. Scale-Free Coherence Profiles

Let the effective gravitational potential be identified with the projected coherence field: $\varphi_{\rm eff}(r) = \Phi(r)$. For circular motion,

$$v_{\rm rot}^2(r) = r\left|\frac{d\varphi_{\rm eff}}{dr}\right| = r\left|\frac{d\Phi}{dr}\right|.$$

Outside the baryonic core, the synchronization field is governed by scale-free coherence. The only radial profile with no preferred length scale and nonzero radial flux is logarithmic:

$$\Phi(r) = A\log(r/r_0), \quad \frac{d\Phi}{dr} = \frac{A}{r}, \quad v_{\rm rot}^2 = A.$$

Flat rotation curves therefore follow directly from scale-free synchronization, with no tuning.

31.2. The Square-Root Coherence Response

To connect A to baryonic matter, define the total baryonic source strength $M_b = \int \rho_b\, d^3x$ and the total coherence charge Q_Φ. The minimal assumption is $Q_\Phi \propto M_b$. The amplitude A of the logarithmic coherence profile is set by the radial flux at the baryonic radius, which under scale-free synchronization satisfies

$$A \sim Q_\Phi^{1/2} \propto M_b^{1/2}.$$

The square-root exponent arises because A is the amplitude of a logarithmic potential sourced by a coherence charge, and the relationship between source charge and field amplitude for a logarithmic potential is sub-linear. Then

$$v_{\rm rot}^2 = A \propto M_b^{1/2},$$

so that

$$v_{\rm rot}^4 \propto M_b.$$

Proposition 31.1 (Baryonic Tully–Fisher from Scale-Free Synchronization)**.** *Under the minimal synchronization model with logarithmic coherence profile and linear coherence-charge response, the rotation velocity satisfies $v_{\rm rot}^4 \propto M_b$ without a dark matter halo and without an empirical interpolation function.*

31.3. Interpretation

The scaling arises from two independent facts. First, scale-free synchronization forces $d\Phi/dr \sim 1/r$, which immediately implies flat rotation curves. Second, the amplitude A satisfies a square-root response to the baryonic source, giving the Tully–Fisher exponent. The crucial move is the square-root coherence response: without it, the model gives flat curves but not the baryonic scaling. Together, these two properties recover the observed relation purely from synchronization geometry, placing the model in direct empirical competition with both ΛCDM halo models and the MOND interpolation function $\mu(a/a_0)$.

32. Relation to Numerical Cosmology and the Illustris Pipeline

Modern cosmological understanding is strongly shaped by large-scale numerical simulations, most notably the Illustris Project and its successor IllustrisTNG [31, 32], which evolve coupled systems of dark matter, baryonic gas, and feedback processes within the ΛCDM framework using N-body gravity, finite-volume hydrodynamics, and subgrid prescriptions for star formation. The resulting outputs reproduce large-scale structure, galaxy populations, and statistical observables with remarkable fidelity.

The synchronization-based framework differs at a foundational level in its choice of dynamical variables. Rather than evolving particle ensembles, the present model evolves a continuous coherence field $\Phi(x,t)$ governed by equation (9). Standard simulations implement a forward pipeline $(\rho_{\rm DM}, \rho_{\rm baryon}) \to$

particle dynamics → gravitational potential → observables. The synchronization framework replaces particle dynamics with field relaxation: $\rho_{\text{baryon}} \to \Phi \to \varphi_{\text{eff}} \to$ observables. The dominant computational task shifts from N-body integration to the solution of nonlinear elliptic PDEs, which scale with grid resolution rather than particle number.

Proposition 32.1 (Simulation Equivalence Test)**.** *Let ρ_b be a baryonic density field obtained from a ΛCDM simulation. If there exists a parameter set for the synchronization field such that the resulting φ_{eff} reproduces both the simulated rotation curves and lensing maps, then the coherence framework provides an observationally equivalent description of the gravitational dynamics.*

32.1. Benchmark Case Study: Reconstructing a Simulated Halo Without Dark Matter

Given $\rho_b(x)$ extracted from Illustris, the standard pipeline computes $\nabla^2\varphi_{\text{tot}} = 4\pi G(\rho_b + \rho_{\text{DM}})$. In the synchronization framework, one instead solves

$$-\nabla \cdot (D(\Phi)\nabla\Phi) + \alpha\Phi^3 - \beta\Phi = \gamma\rho_b(x), \quad (10)$$

then defines $\varphi_{\text{eff}} = \varphi_b + \lambda_1\Phi + \lambda_2|\nabla\Phi|^2$, and computes $v_c(r) = \sqrt{r\, d\varphi_{\text{eff}}/dr}$ and $\kappa(x_\perp) \propto \nabla^2_\perp \varphi_{\text{eff}}$. The reconstruction succeeds if flat rotation curves emerge at large radii without ρ_{DM}, lensing convergence maps reproduce the amplitude and spatial distribution of the simulated signal, and the inferred $\Phi(x)$ exhibits extended structure beyond the baryonic distribution, effectively mimicking a halo.

Remark 32.2. *This procedure does not claim that dark matter is absent at a fundamental level. Rather, it shows that its phenomenological role may be realized by an emergent field degree of freedom. Distinguishing between these possibilities requires observables sensitive to dynamical response, not merely static structure.*

33. Comparative Predictions Across Cosmological Frameworks

We compare three classes of models: ΛCDM with cold dark matter, Modified Newtonian Dynamics (MOND) [34], and the constrained-field synchronization model developed here. The comparison is restricted to qualitative structure, scaling relations, and observable dependencies.

33.1. Rotation Curves

In ΛCDM, flat rotation curves are produced by halo mass profiles and the dependence on baryons is indirect via halo formation. In MOND, the low-acceleration scaling is imposed as a fundamental relation through the universal scale a_0, with low scatter predicted. In the synchronization framework, flat curves emerge from Φ coherence coupling, the dependence on baryons is direct through the source term in equation (9), and low scatter emerges if Φ equilibrates with ρ_b.

33.2. Gravitational Lensing

ΛCDM sources lensing from total mass and naturally accommodates mass-light offsets through collisionless dark matter. MOND requires a relativistic extension for lensing and generally underpredicts cluster lensing strength. The synchronization model sources lensing from $\varphi_{\text{eff}}[\Phi, \rho_b]$; offsets between baryonic matter and lensing centers arise from finite relaxation time of Φ, and cluster lensing strength must arise from the extended field structure.

33.3. Structure Formation

ΛCDM seeds structure through dark matter seeds with a well-developed halo mass function and filamentary cosmic web. MOND produces structure less naturally. The synchronization model generates early growth through coupled Φ–baryon instability, filaments as Φ coherence domain boundaries, and halo universality emerging from the PDE structure of equation (9).

33.4. Dynamical Memory

Only the synchronization framework generically predicts finite relaxation of the gravitational response. ΛCDM shows collisionless relaxation with no memory of prior trajectory classes. MOND is effectively instantaneous. The synchronization model allows observable lag and hysteresis, making it the only framework that predicts correlations between current gravitational response and prior dynamical history.

33.5. Discriminating Observables

Three classes of observation can distinguish the models without parameter fitting. Offset systems such as merging clusters distinguish ΛCDM (persistent mass-light separation from collisionless

dark matter) from MOND (struggles without additional fields) from the Φ-model (separation only if Φ has finite relaxation time). Galaxy rotation scaling relations are exact in MOND, emergent with scatter in ΛCDM, and emergent if Φ equilibrates in the synchronization model. Time-dependent lensing or dynamics are absent from ΛCDM and MOND but generically predicted by the Φ model through lag between baryonic motion and effective gravitational response.

34. Observational Strategy for Detecting Field Relaxation

A distinguishing feature of the synchronization framework is that the effective gravitational response is mediated by a dynamical field $\Phi(x,t)$ with finite relaxation time. We outline observational strategies to detect such relaxation using existing and near-term datasets.

34.1. Merging Galaxy Clusters

Merging clusters provide the cleanest test. In systems such as the Bullet Cluster [35], X-ray observations trace collisional gas while lensing maps the effective mass distribution. Three regimes can be distinguished: ΛCDM predicts lensing peaks tracking collisionless dark matter with persistent offset from baryonic gas; instantaneous modified gravity predicts lensing closely following baryonic mass; the synchronization field predicts lensing remaining offset from baryons temporarily if Φ has not yet relaxed to the new baryonic configuration. A systematic survey of merging clusters at different merger stages can therefore test for time-dependent alignment between baryonic and lensing peaks.

34.2. Time-Resolved Strong Lensing

Strong lensing systems with variable sources provide a complementary probe. If Φ evolves on observable timescales, time-delay measurements taken at different epochs may show systematic shifts not attributable to source variability alone, and lens models reconstructed from different epochs may require slightly different effective potentials even when baryonic structure appears unchanged.

34.3. Galaxy Rotation During Transients

Galaxies undergoing rapid baryonic reconfiguration—starbursts, feedback-driven outflows, tidal interactions—offer a dynamical test. Transient deviations from equilibrium rotation profiles may persist longer than expected from baryonic evolution alone, and hysteresis effects may appear in which the rotation curve depends on recent history rather than only current mass distribution.

34.4. Large-Scale Structure Evolution

On cosmological scales, programs such as the Dark Energy Survey and the Euclid mission measure clustering statistics, growth rates, and weak lensing shear fields. A finite relaxation time for Φ would manifest as scale-dependent deviations in growth rates, mild decorrelation between baryonic tracers and lensing fields, and evolution-dependent bias between observed structure and inferred gravitational potential.

34.5. A No-Go Result for Instantaneous Gravitational Response

We formalize the distinction between instantaneous and dynamical response.

Definition 34.1 (Instantaneous Response Model)**.** *A gravitational model has instantaneous response if $\varphi_{\text{eff}}(x,t) = \mathcal{G}[\rho_b(\cdot,t)](x)$ for some functional $\mathcal{G}$, with no dependence on prior history.*

Definition 34.2 (Dynamical Response Model)**.** *A model has dynamical response if φ_{eff} depends on the history $\{\rho_b(\cdot,s)\}_{s\le t}$ with $\partial_t \mathcal{H} \neq 0$ even when ρ_b is held fixed.*

Proposition 34.3 (No Persistent Lag in Instantaneous Models)**.** *In any instantaneous response model, two systems with identical baryonic configurations at time t must have identical effective potentials at time t. Persistent lag or hysteresis correlated with evolutionary history cannot arise without explicit additional state variables.*

Proof. By definition $\varphi^{(1)}_{\text{eff}}(\cdot,t) = \mathcal{G}[\rho^{(1)}_b(\cdot,t)]$ and $\varphi^{(2)}_{\text{eff}}(\cdot,t) = \mathcal{G}[\rho^{(2)}_b(\cdot,t)]$. If $\rho^{(1)}_b(\cdot,t) = \rho^{(2)}_b(\cdot,t)$, then $\varphi^{(1)}_{\text{eff}} = \varphi^{(2)}_{\text{eff}}$. Observed differences correlated with prior trajectories are therefore inadmissible within this class. □

Corollary 34.4 (Hysteresis as Evidence of Dynamical Fields)**.** *If there exist systems with indistinguishable baryonic configurations at time t but measurably different gravitational responses correlated with evolutionary history, then no instantaneous response model*

can account for the observations. Such behavior requires a dynamical mediating field or additional hidden degrees of freedom.

Remark 34.5. *This result does not distinguish between dark matter and dynamical-field interpretations. It establishes only that any theory reproducing persistent lag must include additional state variables beyond the instantaneous baryonic configuration. In ΛCDM these are collisionless matter components; in the present framework they are encoded in the evolving field Φ. In this sense, gravitational dynamics can be tested for Markovianity.*

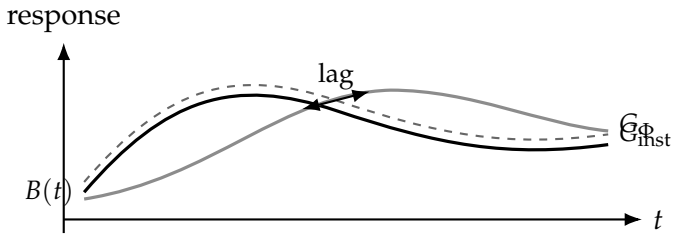

Figure 8: Instantaneous response G_{inst} tracks the baryonic tracer $B(t)$ exactly; the dynamical Φ-field response G_Φ exhibits finite lag. The no-go proposition shows this distinction is structurally unavoidable.

34.6. Falsification Protocol

The following protocol operationalizes the no-go result without assuming a specific model. For each system k at epoch t, measure a baryonic tracer $B_k(x,t)$ (stellar light or gas density) and a gravitational proxy $G_k(x,t)$ (lensing convergence or kinematic potential). Construct pairs (k,ℓ) with $\|B_k(\cdot,t) - B_\ell(\cdot,t)\| \leq \varepsilon$ for an observational tolerance ε. Define the gravitational mismatch $\Delta_{k\ell} := \|G_k(\cdot,t) - G_\ell(\cdot,t)\|$. Evaluate whether $\Delta_{k\ell}$ exhibits systematic dependence on independent indicators of recent evolution (merger stage, starburst activity, gas disturbance) after controlling for redshift, environment, and resolution.

If $\Delta_{k\ell} \approx 0$ for all matched pairs, results are consistent with instantaneous response. If $\Delta_{k\ell}$ is nonzero and correlates with indicators of past dynamical activity, this constitutes evidence of history dependence in the gravitational response. The protocol probes a structural property—memory versus instantaneity—and is therefore model-independent at the level of hypothesis testing.

35. Limitations and Open Problems

The framework presented here is intentionally minimal and operates at the level of effective field theory. Several significant limitations and open problems remain across the four layers of the paper.

Effective field description. The fields Φ, $\mathbf{v}$, and $\mathcal{S}$ are coarse-grained effective variables and do not uniquely determine microscopic configurations. The derivation of the free-energy functional $\mathcal{F}$ from a specific microscopic model remains open for most systems of interest. Similarly, the memory operators $\mathcal{K}_\Phi$, $\mathcal{K}_{\mathbf{v}}$, $\mathcal{K}_{\mathcal{S}}$ introduced in Section 8 are phenomenological; their rigorous derivation from projection operator methods or memory function formalisms would substantially strengthen the framework.

Accessibility collapse and calibration. The term $-\beta(\Phi)\mathcal{S}$ in equation (7) is the most mechanically novel element of the framework. Its quantitative calibration against experimental relaxation data has not been performed, and the functional form of $\beta(\Phi)$ is taken as monotone increasing without further specification. Whether β depends on additional fields, on the history $\mathcal{M}$, or on spatial gradients of Φ is an open question whose answer would determine whether the collapse dynamics belong to a known universality class.

Derived sheaf truncation. Section 12 treats the configuration sheaf as a 1-sheaf in the low-accessibility regime and notes that the high-accessibility regime requires a derived stack with nontrivial higher gluing data. The precise conditions under which the truncation from a derived sheaf to a 1-sheaf is valid, the nature of the higher morphisms encoding trajectory memory, and the connection to existing derived algebraic geometry remain to be developed. In particular, the relationship between the memory kernels $\mathcal{M}_i$ and the $(\infty,1)$-categorical structure of $\mathcal{C}_{\text{adm}}$ requires rigorous treatment.

Reconstruction and inverse problems. The reconstruction of $\mathcal{X}$ from experimental projections $\{\Pi_k[\mathcal{X}]\}$ is an ill-posed inverse problem in general. The forward model is well-defined, but the regularization required for stable inversion—particularly in the presence of higher sheaf obstructions—is

not specified. The admissibility log simulator described in Appendix A provides a forward model but not an inversion scheme.

Cosmological coupling and lensing constraints. The closure relation $\Delta\Phi - m^2\Phi + \lambda\Phi^3 = \alpha\rho_b + \gamma|\nabla\Phi|^2$ contains six free parameters $\{A, B, \alpha, m^2, \lambda, \gamma\}$ that must be fit simultaneously to rotation curves and lensing observables. No such fit has been performed. In particular, the simultaneous reproduction of weak lensing shear correlations and the cluster-scale lensing convergence — the hardest constraint from the Bullet Cluster geometry — has not been demonstrated. Failure on this constraint would falsify the closure relation as stated and require a modified coupling between Φ and the effective metric.

Relativistic consistency at strong curvature. The derivation of the effective metric in Section 17 operates in the weak-field perturbative regime. Whether the synchronization framework extends consistently to strong-field regimes — compact objects, black holes, gravitational wave generation — has not been examined. The stress-energy tensor $T_{\mu\nu}^{\Phi,\mathbf{v},\mathcal{S}}$ appearing in the modified Einstein equations is not fully specified, and its positivity properties (required for energy conditions) are not verified.

Recency optimality beyond exponential decay. The recency optimality proposition of Section 21 is proved under an exponential decay condition on constraint evolution. Whether power-law decay or other non-exponential memory structures — which arise in systems exhibiting scale-free dynamics or long-range correlation — can be handled within the same framework requires extension of the result. The relationship between the memory kernel $K_i(t-s)$ of Section 7 and the optimal truncation of the admissibility log is not worked out in general.

Socio-technical calibration. The modular externalization section of Section 20 provides a formal structure but no quantitative predictions. The conditions under which admissible residues generate genuinely new trajectory classes, as opposed to merely expanding the volume within existing classes, require a theory of combinatorial accessibility growth that is not developed here.

These limitations define the frontier of the framework. The most decision-critical open problem for the paper's primary claims is the cosmological lensing constraint: simultaneous fit of rotation curves and lensing from a single $\Phi[\rho_b]$ without dark matter is the make-or-break test for the synchronization extension.

36. Conclusion: From Structure to Constrained Trajectories

We have argued that mesoscale systems across soft matter physics, biophysics, nanotechnology, and materials engineering share a common mathematical structure. By representing these systems through a coupled field $\mathcal{X}(x,t) = (\Phi, \mathbf{v}, \mathcal{S})$, we obtain a unified description in which structure, transport, and configurational accessibility are intrinsically linked.

Within this framework, self-assembly is reinterpreted as constrained exploration of configuration space. Structure emerges as a field encoding correlations and admissibility, while transport arises as motion constrained by this field and feeds back into it through the coupling term $\mu'(\Phi)|\mathbf{v}|^2$. Interfaces act as active boundaries whose stability arises from the local suppression of configurational accessibility. Dynamics are understood as trajectories through configuration space, and functional behavior corresponds to the stabilization of those trajectories in low-$\mathcal{S}$ basins.

The introduction of trajectory-aware representation extends this picture by incorporating non-Markovian memory and cross-scale consistency. Systems are no longer described solely by their instantaneous configurations, but by overlapping patches of reconstructible trajectories. The Wilson façade structure provides the conceptual foundation for this move: the patchwork of locally valid descriptions, with handoff conditions at the seams, is not an approximation of a hidden global theory but the operative structure of physical description itself.

The configurational accessibility field $\mathcal{S}$ provides the central unifying quantity. It measures the local density of admissible trajectories and governs both the exploration and restriction of configuration space. The term $-\lambda\mathcal{S}$ in the free-energy functional drives the system toward configurations with many admissible futures, while the dynamical term $-\beta(\Phi)\mathcal{S}$ encodes the irreversible collapse of accessibility induced by increasing constraint. The competition between these two tendencies governs the transient accessibility landscape and determines which regions of configura-

tion space remain reachable. In particular, regions that transiently increase in Φ experience accelerated accessibility collapse, making such fluctuations self-reinforcing and driving the system toward locally irreversible organization.

This geometric picture admits a natural topological refinement. As constraints accumulate, not only does the volume of accessible trajectories decrease, but the number of admissible homotopy classes contracts. Structured evolution therefore corresponds to a joint reduction in geometric accessibility and topological diversity. Novelty corresponds to structured accessibility reduction; compression corresponds to the elimination of entire classes of trajectories. Functional systems arise when this process stabilizes: trajectories become confined to a small number of homotopy classes, and perturbations no longer induce transitions between them.

> Function corresponds to confinement within a restricted set of admissible trajectory classes.

From this perspective, design can be interpreted as the controlled induction of accessibility collapse along targeted trajectories: not the imposition of structure directly, but the progressive removal of alternative futures until only the desired evolution remains dynamically admissible. Processes such as cross-linking, crystallization, alignment, and templating are mechanisms for inducing this collapse in targeted regions of configuration space. Biological systems achieve similar effects through sequence-encoded folding pathways and cooperative assembly.

Mesoscale matter is therefore not defined by what it is, but by how it evolves under constraint. Structure, transport, and function are different expressions of the same underlying process: the structured collapse of possibility space. Geometry emerges as the minimal global structure required to represent a sheaf of admissible configurations once higher cohomological obstructions have vanished.

Mesoscale systems are not merely structured—they are structured in motion. Understanding them requires tracing the constrained trajectories through which configurations emerge, and identifying the accessibility and homotopy collapse that render those trajectories stable enough to be called functional.

A. Algorithms for the Admissibility Log Simulator

This appendix describes three algorithms that implement the admissibility log as an executable object, grounding the formal constructions of Sections 8 and 9 in a concrete computational procedure. The algorithms are presented as structured pseudocode; an Abraxas-compatible numerical implementation follows the same structure directly.

A.1. Algorithm 1: RSVP Field Initialization and Event Application

The system state is a tuple $(\Phi, \mathbf{v}, \mathcal{S}, R)$ defined on a discrete spatial grid of width W and height H, where R denotes the residue field accumulating gluing obstruction. Fields are initialized as $\Phi = 0$, $\mathbf{v} = 0$, $\mathcal{S} = \mathcal{S}_0$ for a baseline accessibility $\mathcal{S}_0 \in (0, 1)$, and $R = 0$.

A discrete event $e = (x, y, \Delta\Phi, \Delta\mathbf{v}, \Delta\mathcal{S})$ is applied by a Gaussian kernel of width σ:

$$w_{ij} = \exp\left(-\frac{(i-y)^2 + (j-x)^2}{\sigma^2}\right).$$

Each field component is updated pointwise: $\Phi_{ij} \leftarrow \Phi_{ij} + w_{ij}\Delta\Phi$, and similarly for $\mathbf{v}$ and $\mathcal{S}$. The residue field accumulates the magnitude of the structural update: $R_{ij} \leftarrow R_{ij} + |w_{ij}\Delta\Phi|\,\rho$ for a residue coupling $\rho > 0$. The Gaussian smearing ensures that discrete events approximate localized field operators, so that the continuum limit $\Delta t \to 0$ recovers the RSVP evolution equations.

A.2. Algorithm 2: RSVP Relaxation Step

Between events, the field evolves by a single relaxation step that approximates the coupled PDE dynamics. Spatial gradients of Φ are estimated by finite differences:

$$(\nabla\Phi)_x \approx \frac{\Phi_{i,j+1} - \Phi_{i,j-1}}{2}, \qquad (\nabla\Phi)_y \approx \frac{\Phi_{i+1,j} - \Phi_{i-1,j}}{2},$$

using periodic boundary conditions. The transport field is updated by gradient alignment: $\mathbf{v} \leftarrow \mathbf{v} + \alpha_v \nabla\Phi$, implementing the admissible flux condition that transport follows structural constraint gradients.

The accessibility field evolves by the collapse equation: the effective collapse rate $\beta_{ij} = \beta_0 + \beta_1 \max(\Phi_{ij}, 0)$ encodes the state-dependent feedback $\beta'(\Phi) > 0$, so that ordered regions suppress accessibility faster. The update is $\mathcal{S}_{ij} \leftarrow \mathcal{S}_{ij} + \alpha_\Phi |\mathbf{v}_{ij}|^2 - \beta_{ij}\mathcal{S}_{ij}$, where the first term is transport-induced diversification and the second is constraint-induced collapse.

The structural field diffuses by a discrete Laplacian: $\Phi \leftarrow (1-\epsilon)\Phi + \epsilon\,\bar{\Phi}$, where $\bar{\Phi}$ denotes the local spatial average. This implements the coarse-graining pushforward $\pi_*\mathcal{F}$ at the level of the scalar field. Field values are clipped to $[-1, 1]$ for Φ and $[0, 1]$ for $\mathcal{S}$.

A.3. Algorithm 3: Gluing Obstruction Estimation

The sheaf gluing obstruction is estimated by a patch-based mismatch computation. The spatial domain is covered by overlapping square patches of side length ℓ with stride $s < \ell$, so that neighboring patches overlap in a strip of width $\ell - s$. For each patch, the local mean $\bar{\Phi}_{\text{patch}}$ is computed. The local gluing mismatch at each grid point is

$$\delta_{ij} = |\Phi_{ij} - \bar{\Phi}_{\text{patch}(i,j)}|,$$

where patch(i, j) denotes the patch containing grid point (i, j). Multiple overlapping patches contribute independently, and contributions are averaged. The result is added to the residue field: $R_{ij} \leftarrow R_{ij} + \mu\, \delta_{ij}$, where $\mu > 0$ is a gluing weight. A large R at a grid point indicates high local inconsistency between patches, corresponding to a nontrivial Čech cochain $[\delta] \in \check{H}^1(\{U_i\}, \mathcal{F})$.

A.4. Visualization Interpretation

The output of a simulation run is a sequence of frames, each containing the current values of Φ, $\mathbf{v}$, $\mathcal{S}$, and R. A natural color encoding assigns the red channel to the gluing residue R (obstruction intensity), the green channel to structural order Φ (shifted to $[0, 1]$), and the blue channel to configurational accessibility $\mathcal{S}$. In this encoding, regions of high structural order and low accessibility appear green with suppressed blue, corresponding to functional lock-in; regions of high residue and disordered structure appear red, corresponding to gluing failure; and regions of balanced accessibility appear with prominent blue, corresponding to exploratory dynamics. The vector field $\mathbf{v}$ may be overlaid as a flow visualization to show transport pathways and their alignment with structural constraint gradients.

B. Algorithm for the Cosmological Synchronization Forward Model

This appendix section describes the numerical procedure for the cosmological synchronization forward model of Section 24. The algorithm maps a baryonic density field to effective gravitational observables via the synchronization field Φ, without invoking dark matter as an explicit particle component.

B.1. Algorithm 4: Synchronization Field Solver

Input: a baryonic density field $\rho_b(x)$ on a three-dimensional grid of spacing h. Parameters: coherence decay scale m^{-1}, baryonic coupling α, saturation coefficient λ, gradient reinforcement γ, relaxation step η, convergence tolerance δ_{tol}.

Initialize $\Phi^{(0)} = 0$ on the grid. At each iteration n, compute the discrete Laplacian $\Delta\Phi^{(n)}$ by finite differences with periodic or zero boundary conditions, and the squared gradient magnitude $|\nabla\Phi^{(n)}|^2$ from centered differences. The residual is

$$r^{(n)} = \Delta\Phi^{(n)} - m^2\Phi^{(n)} + \lambda(\Phi^{(n)})^3 - \alpha\rho_b - \gamma|\nabla\Phi^{(n)}|^2.$$

Update $\Phi^{(n+1)} = \Phi^{(n)} + \eta\, r^{(n)}$. Clip values to a physically admissible range $[-\Phi_{\max}, \Phi_{\max}]$. Iterate until $\|r^{(n)}\|_\infty < \delta_{\text{tol}}$.

B.2. Algorithm 5: Effective Potential and Observable Construction

Given a converged field $\Phi(x)$:

Compute the effective gravitational potential $\varphi_{\text{eff}} = A\Phi + B|\nabla\Phi|^2$.

For rotation curves: extract a radial profile $\varphi_{\text{eff}}(r)$ from the cylindrically averaged potential and compute $v_c(r) = \sqrt{r\, d\varphi_{\text{eff}}/dr}$ by numerical differentiation.

For lensing: project the potential along the line of sight to obtain $\psi_{\text{lens}}(x_\perp) = (2/c^2) \int \varphi_{\text{eff}}\, dz$. Then compute convergence $\kappa = \frac{1}{2}\nabla_\perp^2 \psi_{\text{lens}}$ and shear components $\gamma_1 = \frac{1}{2}(\partial_x^2 - \partial_y^2)\psi_{\text{lens}}$ and $\gamma_2 = \partial_x\partial_y\psi_{\text{lens}}$ by finite differences on the projected grid.

For the effective dark matter analog: define $\rho_{\text{eff}} = (4\pi G)^{-1}\Delta\varphi_{\text{eff}}$ and compare its spatial distribution to the dark matter halo inferred from the standard simulation. Agreement indicates that the coherence field reproduces the gravitational role of dark matter from baryonic sources alone.

B.3. Calibration and Falsification Criterion

Fit the six parameters $\{A, B, \alpha, m^2, \lambda, \gamma\}$ to a training set of galaxies with measured rotation curves and lensing profiles. The model is validated only if a single parameter set simultaneously reproduces rotation, weak lensing shear, and cluster convergence maps across independent test systems. Failure on any one observable class falsifies the closure relation equation (9). The strongest test is the Bullet Cluster geometry [35]: the forward model must produce a lensing centroid offset from the baryonic X-ray centroid without invoking collisionless particles.

C. BNF Specification for the Synchronization-Field Simulator

This appendix gives a formal grammar for specifying numerical simulations of the five-dimensional Ising synchronization model. The grammar is written in Backus–Naur form and defines a compact configuration language for simulations of $\sigma : \mathbb{R}^3 \times \mathbb{R} \times \Xi \to \{-1, +1\}$.

C.1. Grammar

```
<simulation>  ::= "simulation" <id> "{" <body> "}"
<body>        ::= <domain> | <field> | <initialization>
                | <dynamics> | <projection>
                | <observables> | <output> | <body> <body>
```

```
<domain>      ::= "domain" "{" "space" "=" <grid3> ";"
                  "time" "=" <timegrid> ";"
                  "internal" "=" <internalgrid> ";"
                  "boundary" "=" <boundary> ";" "}"
<grid3>       ::= "(" <int> "," <int> "," <int> ")"
<timegrid>    ::= "(" <real> "," <real> "," <real> ")"
<internalgrid>::= "(" <int> ")"
<boundary>    ::= "periodic" | "reflecting" | "open"
<field>       ::= "field" "{" "sigma" ":" "ising5d" ";"
                  "phi" ":" "projection" ";"
                  "v" ":" "gradient" ";"
                  "S" ":" "accessibility" ";" "}"
<init>        ::= "initialize" "{" "sigma" "=" <initrule> ";"
                  "seed" "=" <int> ";" "}"
<initrule>    ::= "random" | "biased" "(" <real> ")"
                | "baryon_seeded" "(" <id> ")"
                | "domain_seeded" "(" <int> ")"
<dynamics>    ::= "dynamics" "{" "update" "=" <rule> ";"
                  "steps" "=" <int> ";"
                  "relaxation" "=" <real> ";" "}"
<rule>        ::= "majority" | "metropolis"
                | "heatbath" | "deterministic_sync"
<projection>  ::= "projection" "{"
                  "phi" "=" "mean_internal(sigma)" ";"
                  "v" "=" "negative_gradient(phi)" ";"
                  "S" "=" "log_variance_internal(sigma)" ";" "}"
<observables> ::= "observables" "{" <obs_list> "}"
<obs_list>    ::= <obs> | <obs> <obs_list>
<obs>         ::= "rotation_curve" ";"
                | "lensing_convergence" ";"
                | "coherence_length" ";"
                | "gluing_residue" ";"
<output>      ::= "output" "{" "format" "=" <fmt> ";"
                  "path" "=" <string> ";"
                  "cadence" "=" <int> ";" "}"
<fmt>         ::= "json" | "csv" | "hdf5" | "frames"
```

C.2. Operational Semantics

A simulation state is the tuple $\mathcal{S}_n = (\sigma_n, \Phi_n, \mathbf{v}_n, \mathcal{S}_n, t_n)$. A single update step $\mathcal{S}_n \to \mathcal{S}_{n+1}$ is given by:

$$\begin{aligned}
\sigma_{n+1}(x,\xi) &= \operatorname{sign}\Big(\sum_{(x',\xi')\sim(x,\xi)} \sigma_n(x',\xi')\Big),\\
\Phi_{n+1}(x) &= \tfrac{1}{|\Xi|}\sum_{\xi} \sigma_{n+1}(x,\xi),\\
\mathbf{v}_{n+1}(x) &= -\nabla\Phi_{n+1}(x),\\
\mathcal{S}_{n+1}(x) &= \log\big(1+\operatorname{Var}_{\xi}[\sigma_{n+1}]\big),\\
t_{n+1} &= t_n + \Delta t.
\end{aligned}$$

Execution terminates when $t_n \geq T$.

C.3. Invariant Properties

Proposition C.1 (Boundedness)**.** *For all n, $\sigma_n \in \{-1,+1\}$ and therefore $-1 \leq \Phi_n(x) \leq 1$.*

Proposition C.2 (Monotonic Accessibility Collapse)**.** *Under deterministic synchronization, $\mathcal{S}_{n+1}(x) \leq \mathcal{S}_n(x)$ except at domain boundaries.*

Proposition C.3 (Energy Descent)**.** *Define the discrete energy $E_n = -\sum_{\langle i,j\rangle} \sigma_i\sigma_j$. Then $E_{n+1} \leq E_n$.*

C.4. Observable Extraction Pipeline

Rotation curves are computed from the cylindrically averaged potential: $v_{\text{rot}}(r) = \sqrt{r\,|d\Phi/dr|}$. The effective density analogue is $\rho_{\text{eff}}(x) = -\Delta\Phi(x)$. Lensing convergence is $\kappa(x_\perp) \propto \int \Delta_\perp \Phi\, dz$. The coherence length is $\xi_c = \int r\, C(r)\, dr$ where $C(r) = \langle \Phi(x)\Phi(x+r)\rangle$.

C.5. Computational Complexity

For grid size N^3 and internal dimension M, the update cost per step is $\mathcal{O}(N^3M)$, gradient computation is $\mathcal{O}(N^3)$, and total runtime is $\mathcal{O}(TN^3M)$. This scaling is linear in the internal dimension, making high-dimensional synchronization computationally tractable on modern GPU hardware.

D. Reference Implementation of the Synchronization Model

D.1. Data Layout

We discretize space as a cubic lattice of size N^3 with internal dimension M. The primary state is $\sigma \in \{-1,+1\}^{N\times N\times N\times M}$, stored as a flattened array with row-major indexing $\texttt{idx} = (((x\cdot N + y)\cdot N + z)\cdot M + \xi)$, ensuring coalesced memory access along the internal dimension. Derived fields $\Phi \in \mathbb{R}^{N^3}$, $\mathbf{v} \in \mathbb{R}^{N^3\times 3}$, and $\mathcal{S} \in \mathbb{R}^{N^3}$ are computed from σ at each step.

D.2. Parallel Update Kernel

Each thread updates one site (x,y,z,ξ) by majority vote over all neighbors in the 3D spatial stencil and both internal neighbors:

$$\begin{aligned}
\texttt{sum} = &\sum_{(dx,dy,dz)\in\{\pm1,0\}^3\setminus\{0\}} \sigma[x{+}dx, y{+}dy, z{+}dz, \xi]\\
&+ \sigma[x,y,z,\xi{+}1] + \sigma[x,y,z,\xi{-}1],\\
\sigma_{\text{new}}[x,y,z,\xi] &= \operatorname{sign}(\texttt{sum}).
\end{aligned}$$

D.3. Projection Kernels

The three derived fields are computed from σ by independent parallel reductions. The mean over ξ gives Φ; centered finite differences give $\mathbf{v} = -\nabla\Phi$; and the log-variance over ξ gives $\mathcal{S}$. The effective potential is computed as $\varphi_{\text{eff}} = \Phi$ in the minimal model, or $\varphi_{\text{eff}} = A\Phi + B|\nabla\Phi|^2$ in the full closure model. Rotation curves follow from radial differentiation of the cylindrically averaged φ_{eff}, and lensing convergence from line-of-sight projection and transverse Laplacian.

E. Continuum Limit of the Synchronization Dynamics

E.1. Coarse-Graining

Define the coarse-grained field $\Phi(x,t) = (1/M)\sum_\xi \sigma(x,t,\xi)$ and assume local spatial

averaging over scale ϵ: $\Phi_\epsilon(x) = \int K_\epsilon(x-y)\Phi(y)\,dy$.

E.2. Expansion of the Update Rule

The discrete synchronization update $\sigma^{n+1} = \operatorname{sign}(\sum_{\text{nbrs}} \sigma^n)$ can be approximated as $\sigma^{n+1} \approx \tanh(\beta\Delta\sigma^n)$. Expanding for small gradients and projecting onto the mean field gives:

Theorem E.1 (Continuum Limit)**.** *The discrete synchronization model converges, under coarse-graining, to a reaction–diffusion system of Ginzburg–Landau type:*

$$\partial_t \Phi = D\Delta\Phi - \lambda\Phi^3 + \eta,$$

with coupled transport $\mathbf{v} = -\nabla\Phi$ *and accessibility* $\partial_t \mathcal{S} = -\alpha\Phi^2$.

Sketch. Averaging $\tanh(\beta\Delta\sigma^n)$ over the internal dimension and expanding tanh to cubic order yields $\partial_t\Phi \approx D\Delta\Phi - \lambda\Phi^3 + \eta$, where D and λ are determined by the lattice geometry and η encodes residual fluctuations. The accessibility equation follows from $\partial_t \operatorname{Var}_{\tilde{\varsigma}}[\sigma] \propto -\Phi^2$ under majority-vote dynamics. □

E.3. Emergence of Effective Gravity

Setting $\varphi = \Phi$ and taking the equilibrium limit $\partial_t\Phi = 0$ with $\lambda\Phi^3 \ll D\Delta\Phi$ gives $D\Delta\Phi \approx -\gamma\rho_b$, recovering a Poisson-like equation $\nabla^2\varphi = \rho_{\text{eff}}$. The effective density $\rho_{\text{eff}} = -D^{-1}\gamma\rho_b$ is proportional to baryonic matter, so standard gravitational behavior is recovered in the high-density limit. Deviations arise in the low-density regime where the cubic term $\lambda\Phi^3$ becomes negligible and coherence extends beyond baryonic support, generating the additional effective potential responsible for flat rotation curves and extended lensing.

References

[1] S. Peng, Q. Guo, T. C. Hughes, and P. G. Hartley, In situ synchrotron SAXS study of polymerizable microemulsions, *Macromolecules* **44**, 3007–3015 (2011).

[2] K. M. Weigandt, L. Porcar, and D. C. Pozzo, In situ neutron scattering study of structural transitions in fibrin networks under shear deformation, *Soft Matter* **7**, 9992 (2011).

[3] G. M. Newbloom, F. S. Kim, S. A. Jenekhe, and D. C. Pozzo, Mesoscale morphology and charge transport in colloidal networks of poly(3-hexylthiophene), *Macromolecules* **44**, 3801–3809 (2011).

[4] H. Afifi, G. Karlsson, R. K. Heenan, and C. A. Dreiss, Wormlike micelles with elliptical cross-section in cholesterol-based surfactants, *Langmuir* **27**, 7480–7492 (2011).

[5] S. S. Pai et al., Conformation of PEG chains in mono-PEGylated proteins, *Bioconjugate Chemistry* **22**, 2317–2323 (2011).

[6] S. Ossowski et al., Aggregation behavior of bovine κ- and β-casein, *Langmuir* **28**, 13577–13589 (2012).

[7] L. Liu et al., Conversion of concentration gradients into mechanical force via core–shell capsules, *J. Phys. Chem. B* **116**, 974–979 (2012).

[8] G. M. Newbloom, K. M. Weigandt, and D. C. Pozzo, Structure and property development of poly(3-hexylthiophene) organogels, *Soft Matter* **8**, 8854 (2012).

[9] S. N. Bhat, R. Di Pietro, and H. Sirringhaus, Electroluminescence in ion-gel gated conjugated polymer transistors, *Chem. Mater.* **24**, 4060–4067 (2012).

[10] K. Larson-Smith and D. C. Pozzo, Pickering emulsions stabilized by nanoparticle surfactants, *Langmuir* **28**, 11725–11732 (2012).

[11] P. Sirohi et al., PEG-like block copolymers self-assemble into stealth nanocarriers, *Advanced Science* **13**, e17048 (2026).

[12] B. Yin et al., Chlorination-controlled aggregation enabling high-efficiency organic solar cells, *Nat. Commun.* **17**, 2340 (2026).

[13] M. Tancredi et al., Structure, flow, and functionality in rhamnolipid systems, *ACS Sustainable Chem. Eng.* **14**, 415–427 (2026).

[14] Z. Ye et al., Interfacial organization of nanoparticles in oil–water systems, *Food Hydrocolloids* **173**, 112255 (2026).

[15] E. Poliukhina et al., Direct measurement of protein interaction potentials, *ACS Nano* **20**, 8487–8497 (2026).

[16] E. Villano et al., Microfluidic production of lipid-polymer nanoparticles for siRNA delivery, *Int. J. Pharmaceutics* **688**, 126440 (2026).

[17] M. Agarwal, R. Schweins, and F. Gröhn, Light-induced structural evolution in electrostatic nanoassemblies, *Polymers* **18**, 190 (2026).

[18] L. Perez-Chirinos et al., Peptide electrostatic modulation of neural cell fate, *Advanced Science* **13**, e07946 (2026).

[19] S. Qian et al., Nanoplastic interactions with biomembranes, *Environ. Sci.: Nano* (2026).

[20] Y. Xu et al., Shear-induced alignment and transport in conjugated polymers, *Advanced Materials* **38**, e21831 (2026).

[21] S. V. R. Akepati et al., Machine-learning analysis of 2D SAXS profiles, *ACS Meas. Sci. Au* **6**, 1–20 (2026).

[22] J. Wong, J. Brousseau, and H. M. Titi, Liquid crystal structure revealed by small-angle scattering, *Small Methods* **10**, e01808 (2026).

[23] F. Vitale et al., SAXS analysis of phase transitions in surfactant systems, *J. Colloid Interface Sci.* **702**, 138966 (2026).

[24] K. Q. K. Truong and A. G. Marangoni, Multi-scale triglyceride crystal network analysis via USAXS, *RSC Adv.* **16**, 12502–12510 (2026).

[25] J. Schmidhuber, A possibility for implementing curiosity and boredom in model-building neural controllers, *Proc. SAB* (1991).

[26] J. Schmidhuber, Developmental robotics, optimal artificial curiosity, creativity, music, and the fine arts, *Connection Science* **18**, 173–187 (2006).

[27] M. Wilson, *Wandering Significance: An Essay on Conceptual Behaviour*, Oxford University Press, Oxford (2006).

[28] M. Wilson, *Physics Avoidance: Essays in Conceptual Strategy*, Princeton University Press, Princeton (2017).

[29] I. W. Hamley, Small angle X-ray scattering of peptides and proteins, *Chem. Soc. Rev.* **52**, 4173–4203 (2023).

[30] J. Gao et al., Controlling self-assembling peptide hydrogel properties through network topology, *Biomacromolecules* **18**, 826–834 (2017).

[31] M. Vogelsberger et al., Introducing the Illustris Project: Simulating the coevolution of dark and visible matter, *Mon. Not. R. Astron. Soc.* **444**, 1518–1547 (2014).

[32] D. Nelson et al., The IllustrisTNG simulations: Public data release, *Mon. Not. R. Astron. Soc.* **475**, 624–647 (2018).

[33] Planck Collaboration, Planck 2018 results. VI. Cosmological parameters, *Astron. Astrophys.* **641**, A6 (2020).

[34] M. Milgrom, A modification of the Newtonian dynamics as a possible alternative to the hidden mass hypothesis, *Astrophys. J.* **270**, 365–370 (1983).

[35] D. Clowe et al., A direct empirical proof of the existence of dark matter, *Astrophys. J. Lett.* **648**, L109–L113 (2006).

[36] V. C. Rubin, W. K. Ford Jr., and N. Thonnard, Rotational properties of 21 SC galaxies with a large range of luminosities, *Astrophys. J.* **238**, 471–487 (1980).

[37] E. Verlinde, Emergent gravity and the dark universe, *SciPost Physics* **2**, 016 (2017).

[38] B. Famaey and S. McGaugh, Modified Newtonian Dynamics (MOND): Observational phenomenology and relativistic extensions, *Living Reviews in Relativity* **15**, 10 (2012).

[39] S. S. McGaugh, F. Lelli, and J. M. Schombert, Radial acceleration relation in rotationally supported galaxies, *Phys. Rev. Lett.* **117**, 201101 (2016).

[40] L. Onsager, Crystal statistics. I. A two-dimensional model with an order-disorder transition, *Phys. Rev.* **65**, 117–149 (1944).

[41] P. C. Hohenberg and B. I. Halperin, Theory of dynamic critical phenomena, *Rev. Mod. Phys.* **49**, 435–479 (1977).

[42] V. Springel et al., Simulations of the formation, evolution, and clustering of galaxies and quasars, *Nature* **435**, 629–636 (2005).

[43] C. W. Misner, K. S. Thorne, and J. A. Wheeler, *Gravitation*, W. H. Freeman (1973).

[44] B. Hoffmann, *Relativity and Its Roots*, Dover Publications (1983).

[45] P. M. Chaikin and T. C. Lubensky, *Principles of Condensed Matter Physics*, Cambridge University Press, Cambridge (1995).

[46] A. Onuki, *Phase Transition Dynamics*, Cambridge University Press, Cambridge (2002).

[47] J. W. Cahn and J. E. Hilliard, Free energy of a nonuniform system. I. Interfacial free energy, *J. Chem. Phys.* **28**, 258–267 (1958).

[48] S. M. Allen and J. W. Cahn, A microscopic theory for antiphase boundary motion, *Acta Metall.* **27**, 1085–1095 (1979).

[49] A. J. Bray, Theory of phase-ordering kinetics, *Adv. Phys.* **43**, 357–459 (1994).

[50] G. M. Whitesides and B. Grzybowski, Self-assembly at all scales, *Science* **295**, 2418–2421 (2002).

[51] C. Storm, J. J. Pastore, F. C. MacKintosh, T. C. Lubensky, and P. A. Janmey, Nonlinear elasticity in biological gels, *Nature* **435**, 191–194 (2005).

[52] L. C. Evans, *Partial Differential Equations*, 2nd ed., American Mathematical Society, Providence (2010).

[53] L. Ambrosio, N. Gigli, and G. Savaré, *Gradient Flows in Metric Spaces and in the Space of Probability Measures*, Birkhäuser, Basel (2008).

[54] A. Hatcher, *Algebraic Topology*, Cambridge University Press, Cambridge (2002).

[55] G. E. Bredon, *Sheaf Theory*, 2nd ed., Springer, New York (1997).

[56] J. Lurie, *Higher Topos Theory*, Princeton University Press, Princeton (2009).

[57] M. Nakahara, *Geometry, Topology and Physics*, 2nd ed., Institute of Physics Publishing, Bristol (2003).

[58] R. M. Wald, *General Relativity*, University of Chicago Press, Chicago (1984).

[59] R. S. Sutton, The bitter lesson, Essay (2019).

[60] A. Vaswani et al., Attention is all you need, *Adv. Neural Inf. Process. Syst.* **30** (2017).

[61] K. Friston, The free-energy principle: A unified brain theory?, *Nat. Rev. Neurosci.* **11**, 127–138 (2010).

[62] M. C. Cross and P. C. Hohenberg, Pattern formation outside of equilibrium, *Rev. Mod. Phys.* **65**, 851–1112 (1993).